On the Astromineralogy of the 13 μm Feature in the Spectra of Oxygen-Rich AGB Stars

A Thesis

submitted to

the Faculty of the Graduate School

University of Missouri-Columbia

In Partial Fulfillment of the Requirements for the Degree

Master of Science

by

Kyle David DePew

Dr. Angela Speck, Advisor

Department of Physics & Astronomy

University of Missouri-Columbia

May 2006

The undersigned, appointed by the Dean of the Graduate School, have examined the thesis entitled

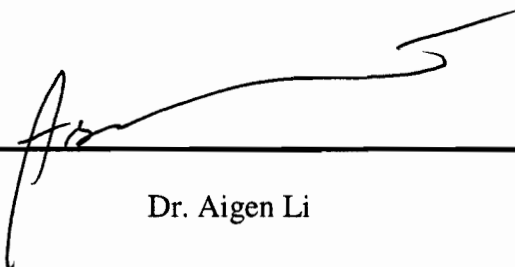ON THE ASTROMINERALOGY OF THE 13 MICRON FEATURE IN OXYGEN-RICH ASYMPTOTIC GIANT BRANCH STARS

Presented by Kyle DePew
A candidate for the degree

MASTER OF SCIENCE

and hereby certify that in their opinion it is worthy of acceptance:

_____

Dr. Angela Speck

_____

Dr. Aigen Li

_____

Dr. Alan Whittington

Abstract

Intermediate-mass stars (0.8-8.0M$_\odot$) are major contributors of new elements to interstellar space. These stars eventually evolve into *asymptotic giant branch* (AGB) stars. During the AGB phase, these stars lose mass to their surroundings, leading to the creation of circumstellar shells of gas and dust. Asymptotic Giant Branch (AGB) Stars have several interesting infrared spectral features.

Approximately half the oxygen-rich AGB stars to be investigated spectroscopically exhibit a feature at $\sim$13 μm. Furthermore, the 13μm feature is associated with semiregular variables (SRs) rather than Miras or red supergiants. While Miras and SRs differ in several ways, with respect to their circumstellar shells, the important difference is that Mira shells are optically thicker than SR shells. Therefore, identification of the 13μm feature provides a diagnostic for the effect of differing circumstellar shell parameters on dust formation.

The carrier of this feature has not yet been unequivocally identified, but has been attributed to various dust species, including corundum (α-Al$_2$O$_3$), spinel (MgAl$_2$O$_4$) and silica (SiO$_2$). In order to constrain the carrier of the 13 μm feature, we have used the 1-d radiative transfer code DUSTY to model the effects of composition and optical depth on the shape and strength of the emerging 13 μm feature from corundum, spinel and quartz grains. We have modeled various abundances of corundum, spinel and quartz together with warm silicate and/or amorphous alumina in dust shells surrounding O-rich AGB stars. These models demonstrate that i) spinel is unlikely to be the carrier of the 13μm feature; ii) if corundum is present in these circumstellar dust shells, even at very low relative abundances, a $\sim$13 μm

feature should be observed; iii) corundum's weak $\sim$21 μm feature will not be observed, even if it is responsible for the $\sim$13 μm feature; iv) corundum grains must be spherical to exhibit the 13μm feature. Other grain shapes (spheroids, ellipsoids, hollow spheres) shift the features to longer wavelengths for both spinel and corundum. v) if silica grains are the carrier of the $\sim$13 μm feature they are unlikely to be either spherical or the polymorph quartz.

More laboratory optical data for the polymorphs of silica are needed to determine whether they are the carrier of the $\sim$13 μm.

Acknowledgements

I would like to thank my advisor, Dr. Angela Speck, for patiently answering my countless questions and for giving me invaluable guidance in the course of my research. I would also like to thank my thesis committee members, Dr. Aigen Li and Dr. Alan Whittington, for graciously giving their time.

Thanks are also due to Dr. Greg Sloan of Cornell University for giving me access to his *ISO* data and to Dr. Anne Hofmeister of Washington University in St. Louis for assistance in finding optical constants. I also wish to thank Dr. Catharinus Dijkstra for the use of his computer program for determining scattering and absorption cross-sections of different grain shapes and sizes.

Without these people this work would have been impossible.

Contents

List of Figures

xiii

Chapter 1: Introduction

This thesis investigates the nature of dust surrounding intermediate-mass evolved stars. This stardust is important because it enriches the interstellar medium with heavy elements and affects galactic chemical evolution. It is also pertinent to star and planet formation and thus the origins of life.

1.1   Background

Several minutes after the Big Bang, the first atoms formed. Most of these atoms were hydrogen and deuterium, but helium also comprised around 20% of the matter. Along with these species, a smaller fraction of lithium was present at this time. Over the next one to two million years, the universe cooled and coalesced into clouds of gas which, through gravitational attraction, came together to form the first stars. It is these stars that gave rise to the modern day universe by their nucleosynthesis of heavier elements.

As a star proceeds through its lifecycle, changes in its temperature and luminosity can be plotted on what is known as the Hertzsprung-Russell (HR) diagram. (See Figure 1.1.) When stars form, they begin their evolutionary path on the HR diagram, moving from the upper right. As they evolve they move towards the so-called main sequence, where the

majority of their lives are spent. While stars spend 90% of their lives in approximately the same position on the HR diagram (on the main sequence), previous and subsequent phases of their lives are marked by enormous changes in their temperatures and luminosities. The track of these changes can be plotted on the HR diagram. Luminosity, or total power output of a star, is governed by the rate of fusion reactions occurring in the core. Because the pressure brought to bear on the core is a result of more mass being attracted to the center, we know that greater luminosity is a result of greater mass. Thus, the main sequence can also be considered as a mass sequence, with less massive stars being found farther down and to the right (cooler and fainter) and more massive ones up and to the left (hotter and brighter).
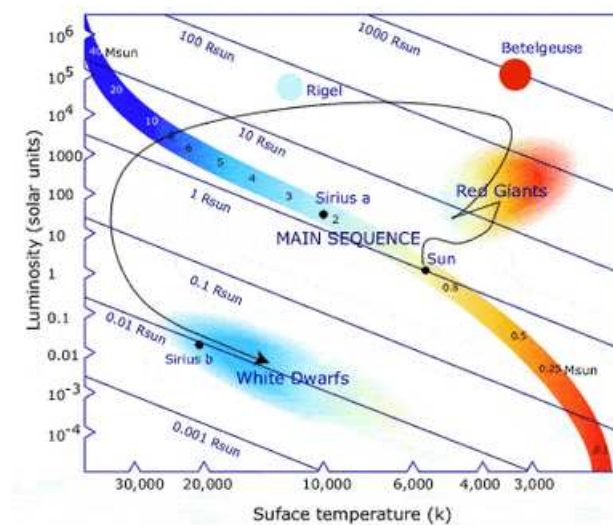
Figure 1.1: *An example of a Hertzsprung-Russell diagram. Note the main sequence line trending from the upper left to the lower right.*

1.2 Stellar Evolution

During the main sequence stars produce energy by fusing hydrogen to make helium. After a star of mass 0.8-8 $M_\odot$ has depleted its core hydrogen supply, gas and radiation pressure decrease and the inner regions of the star contract under the influence of gravity. When this happens, gravitational potential energy is converted into kinetic energy and thus heat. This leads to an ignition of the hydrogen shell surrounding the core, which in turn pushes the exterior layers of the star outward. As these shells expand and cool, the helium core continues to contract. The hydrogen shell continues to burn, dumping more helium ash onto the core.

As more mass falls to the center of the star, the core continues to collapse and becomes denser and hotter. Some of the heat being produced in the hydrogen-burning shell also penetrates the core. As the core becomes compressed to greater and greater densities, its component particles are squeezed into smaller and smaller spaces. By the Pauli Exclusion Principle, no two fermions[1] can occupy the same state. For this reason, the particles resist until there is sufficient energy to excite one or more particles to a higher energy state. This is called degeneracy pressure. A degenerate gas conducts heat easily, so that any additional energy is propagated through the core very rapidly. At about 10^8 K, there is enough energy to overcome the degeneracy pressure. At this point the core begins to burn all at once and an event called the "helium flash" occurs. After the helium flash, the star enters the horizontal branch phase. During this phase, carbon is produced by way of the triple-α process. The triple-α process, also known as the Salpeter process, occurs when three helium nuclei (α

---

[1] A class of particles including protons, electrons and neutrons

particles) collide and fuse, forming a carbon nucleus and releasing energy. Occasionally another α particle will fuse with a carbon nucleus to form oxygen.

1.2.1 The Asymptotic Giant Branch

When the helium in the core has been depleted, the star enters the asymptotic giant branch (AGB) stage of its lifecycle. This stage is so-named because its path along the HR diagram now curves backwards such that it asymptotically approaches the red giant branch preceding it. Here the core of the star is comprised of carbon and oxygen. Further collapse is halted by degeneracy pressure. These elements are never ignited because there is never sufficient energy to do this. Above the core is the helium-burning shell, which in turn is surrounded by a hydrogen-burning shell (see Figure 1.2).
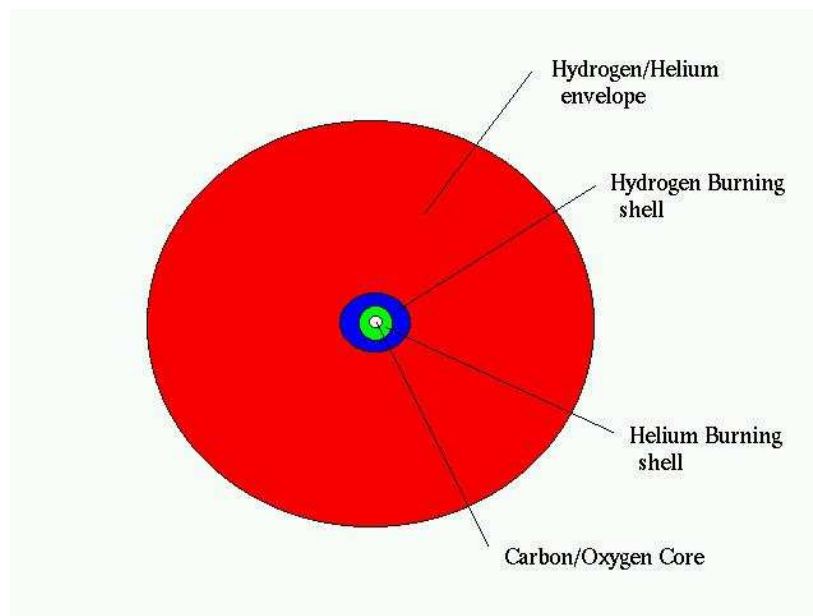
Figure 1.2: *A diagram of the structure of an AGB star.*

Pressure and temperature vary within the hydrogen- and helium-burning shells. The

rate at which reactions occur in these shells is very temperature-dependent. Stars undergo pulsations due to alternating periods of contraction and expansion brought on by heating. Because the star is thermally unstable, the gas attempts in vain to reestablish hydrostatic equilibrium (a balance of gravitational and pressure forces). Meanwhile, the expanding regions cool, increasing the opacity of the interior of the star. Because radiation can no longer propagate through these regions, it is absorbed, heating the opaque matter and causing convection currents to form. These currents dredge carbon, oxygen and other elements from the helium-burning shell up to the surface. By now the outer layers of the star have been pushed out far from the core. Gravity at the surface is sufficiently weak to allow this matter to be expelled. As this matter drifts away from the star it cools. The mass-loss rate can be anywhere from ten to a hundred million times that of the solar wind, but this stellar wind possesses an outflow velocity usually on the order of one-tenth to one-hundredth that of the sun. As a result, matter accumulates and dust can form from the (gaseous) atoms and molecules present in the shell. Because the mass-loss rate increases during the AGB phase, the dust density around the star should increase.

1.2.2 Nucleosynthesis

Within the hydrogen- and helium-burning shells several reactions are now occurring. In the helium-burning shell, the triple-α process continues, but now the *s-process* begins. The *s-process* (slow process) is a process by which neutrons are slowly captured by various elements, usually once every few hundred years (Pagel, 1997). The neutrons required for this process are provided by neon and carbon atoms fusing with helium. Heavier elements up to bismuth

can be created through the *s-process*. Uranium and thorium can only be produced via the *r-process*. The *r-process*, unlike the *s-process*, does not occur in AGB stars, but is worth mentioning here. This process occurs when neutron capture is much more rapid than the β-decay half-life of a nucleus, usually on the order of seconds. This means that massive nuclei build up quickly. The products of the *r-process* differ from those of the *s-process* in the isotopes that form.

Besides the *s*- and *r-processes*, two other processes are important: the p-p chain and the CNO cycle, which both occur in the hydrogen burning shell. The first step in the p-p (proton-proton) chain occurs when two protons collide and fuse, resulting in a deuterium nucleus, a β-particle (in this case a positron) and a neutrino. Within a short time, usually of the order of a second, the new deuterium nucleus combines with another proton, creating a ^{3}He nucleus and a γ ray. Eventually two of these ^{3}He nuclei will collide, ejecting two protons and resulting in a ^{4}He nucleus. The γ rays given off in this reaction provide energy to the core. See Figure 1.3.

In the CNO cycle, carbon acts as a catalyst in the reaction (See Figure 1.4). First, a ^{12}C nucleus captures a proton and emits a γ ray. At this point, the carbon has become ^{13}N. With a half-life of less than ten minutes, this isotope soon beta-decays to ^{13}C. Once again, the carbon captures a proton and emits a γ ray, forming ^{14}N. This nitrogen then captures its own proton and emits another γ ray, creating ^{15}O. Next, ^{15}O beta-decays to ^{15}N, which finally captures another proton and ejects an α-particle, returning a ^{12}C nucleus to the reaction zone. In this way, H is fused to make He. Once again, the γ rays provide energy to the core.
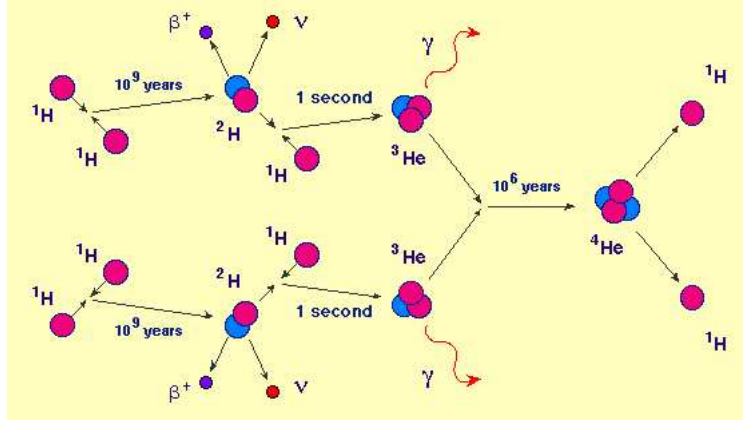
Figure 1.3: *The p-p chain. Here β denotes a β-particle, ν a neutrino, and γ a γ-ray emission. The times noted at the various reactions indicate the average amount of time before the next reaction occurs. Temperatures of about 1.0 x 10^7 K are required to initiate this process. Higher temperatures are necessary for the creation of larger nuclei.*
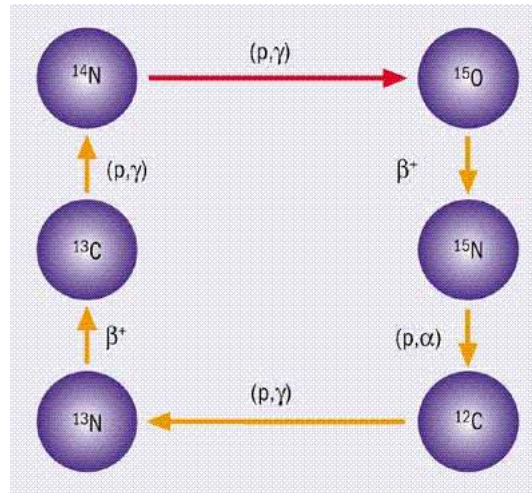
Figure 1.4: *The CNO cycle. Symbols in parentheses denote particles that are gained by the nucleus in the reaction, while β$^+$ indicates positron decay. p denotes a proton and γ a γ-ray emission.*

1.3 Circumstellar Shells

1.3.1 Chemistry

A very important aspect of the circumstellar shell is its carbon to oxygen (C/O) ratio. The cosmic ratio of carbon to oxygen is of the order of C/O $\approx$ 0.4. Therefore, AGB stars are all born oxygen-rich (i.e. there is more oxygen than carbon). It is only later that the convection currents set up within the star dredge up large amounts of carbon and oxygen from the helium-burning shell. If the star is especially efficient at fusing helium into carbon, the C/O ratio can be raised to a value above unity, leading to a carbon-rich star. Because carbon and oxygen have a tendency to form the very stable carbon monoxide molecule (CO) at high temperatures close to the star, one of these two elements is rendered almost completely unavailable for future species formation at greater distances in cooler environments. If, after dredging up material from the helium-burning shell, the C/O ratio rises to 1 or higher, then carbon will dominate the circumstellar chemistry. Conversely, if C/O < 1, oxygen will dominate. For this reason, AGB stars are classified as either carbon-rich (C-rich) or oxygen-rich (O-rich). Only stars between 2 and 4 $M_\odot$ will evolve into C-rich stars. More massive stars engage in hot-bottom burning,[2] which produces more nitrogen at the expense of carbon via the CNO cycle. Less massive stars do not experience sufficient numbers of thermal pulses to enrich the envelope with carbon. In addition to carbon and oxygen,

---

[2]Hot-bottom burning occurs when the hydrogen and helium-burning shells intermingle and products from the triple-α process are fed into the CNO cycle which is taking place in the H-burning shell.

magnesium, iron and silicon[3] are fairly abundant in the gas expelled by AGB stars. Thus the dust is dominated by silicates[4] and oxides. Both of these mineral types form around O-rich stars in large quantities. Aluminum and calcium are also relatively common, though not so much as silicon, magnesium and iron. I shall pass over the C-rich mineralogy, as this thesis will concern itself only with the mineralogy of O-rich stars.

As the star evolves, geometric and optical depth (see § 1.3.3) increase because more matter is ejected. The mass-loss rate increases as the star becomes more unstable and convection currents become more efficient.

1.3.2 Variability

AGB stars show variability in their brightness and color on timescales of days to years. These stars can be divided into classes according to the nature of their variations and generally fall into one of two classes: Mira and semi-regular variable (SR) stars. Miras and SR stars are sometimes difficult to classify. They are not yet entirely understood. Miras generally exhibit a regular amplitude variation; i.e. pulsations of their outer shells resulting in mass loss and changes in magnitude are of fairly predictable duration and amplitude. Semi-regulars, as their name suggests, have varying pulsation periods. Furthermore, the amplitude of pulsation is smaller in SRs than in Miras. The SR class is also further subdivided into SRa, SRb, SRc and SRd divisions, with SRas possessing the least variation in period. As one progresses

---

[3]It should be noted that elements such as magnesium, iron, silicon, aluminum and calcium are present in these stars from birth. Very little of these elements is made in the star compared to the initial amount.

[4]Silicates are compounds of SiO_2 or SiO_4 combined with one or more metals, in this case mostly magnesium and iron.

through the alphabet, the semi-regulars generally increase in the variability of their pulsation periods. There is currently a debate concerning the evolution of these stars. While some argue that SRs evolve into Miras (e.g. Feast & Whitelock 1987), it has also been suggested that stars can experience successive periods in which they could be classified alternately as SRs and Miras (Kerschbaum & Hron 1992). It should also be noted that SRs tend to have dust shells that are optically thinner than those of Miras (e.g. Marengo et al. 2001). This means that there is less matter through which the radiation from a star must pass.

1.3.3 Optical Depth

Optical depth is a measure of the extinction of light as it passes through a material. Greater amounts of dust will scatter or absorb more of the incident radiation and permit fewer photons to pass through unhindered. Wavelengths that are close to resonance in a chemical bond or a valence electron energy level will be more readily absorbed than others. As a result, the scattering and absorption coefficients of a material vary with wavelength. Thus, optical depth is very closely tied to the properties of the medium and grain morphology and is wavelength dependent. It is therefore not necessarily correlated with geometric thickness, which involves the spatial range of a dust shell.

The change in radiative intensity after passing through a distance dx is defined as:

$$dI_\nu = -\kappa_\nu I_\nu dx$$

where κ_ν is the opacity of the grains. Then optical depth is defined as:

$$\tau_\nu = \int_{pathlength} \kappa_\nu \rho dx$$

where ρ is the density of the grains. This quantity is useful in calculating the absorption of radiation A:

$$A = e^{-\tau_\nu}$$

It should be noted that the opacity κ_ν is dependent on a number of factors, such as the mineral composition, crystal structure and grain size and shape.

The complex refractive index is: $m = n - ik$ where n is the real refractive index (which determines the phase velocity of light) and k is the extinction coefficient. Inserting these quantities into the electromagnetic wave equation gives us the outgoing intensity of the radiation. Similar to the optical constants n and k are the scattering and absorption cross-sections, which are calculated using n and k. They are related to the geometric grain cross-sections, but also depend on the wavelength dependent extinction properties of the grain material. These quantities indicate the likelihood of scattering and absorption of a photon at a given wavelength. Because scattering and absorption cross-sections, like surface size, dictate the number of photons that will interact with a dust particle, they have units of area.

1.3.4   The Shapes of Grains

Grain morphology is crucial to understanding the composition of AGB dust shells. In general, grains are classified as either spherical, spheroidal (prolate or oblate; two of the three Cartesian axes are equal), ellipsoidal (all three axes can vary) or porous. Porous (also called "fluffy") grains possess any number of pockets around which the atoms and molecules accumulate. For this reason, they must be modeled such that the optical constants vary from

11

those of the grain material to $n=1$, $k=0$ (for the vacuum) and then back again. Morphology can be determined by several factors, such as the material's sublimation and evaporation temperatures and the density of the dust. There is, for example, a tendency of particles which condense at higher temperatures to form spherical grains as opposed to spheroidal, ellipsoidal or porous grains (Voshchinnikov & Semenov 2000). Therefore, grain formation temperature as well as mineral species is important in dust shell models. For the work presented here, spherical, spheroidal, ellipsoidal and hollow spherical grains are modeled. Though hollow spheres are not expected to form, they are modeled as a proxy for fluffy grains because they represent the simplest example of fluffy grains. Theoretically, a fluffy grain could be modeled as a series of many different spheres that have fused together. For a more in-depth discussion of cross-section and optical constant calculations of these differing grain shapes, see Bohren & Huffman (1983) or Min, Hovenier & de Koter (2003).

Mineral polytypes also affect spectra (See Figure 1.5). Polytypes are the different crystalline structures that a given mineral with a specific elemental formula can take. For example, corundum is also called α-Al_2O_3, indicating alumina crystals with a rhombohedral structure. Al_2O_3 can also form other crystal structures, such as cubic or hexagonal lattices. In addition to crystalline structures, grains can also be amorphous. These compounds do not possess a definite structure or periodic lattice like crystalline materials.

1.3.5 Spectroscopy

We can study the nature of circumstellar dust through three methods: imaging and spectral and meteoritic analysis[5]. Imaging will not be discussed here because it is beyond the scope of the present work. As mentioned above, many factors affect the light frequencies which are transmitted or absorbed and re-emitted by the dust. Due to the unique structure and bonds of each atom or molecule, repulsions and attractions between the particles will vary. When a molecule bends or stretches the bonds between two or more atoms, energy can be emitted in the form of a photon. Each mineral species possesses its own unique set of bonds which will resonate at different wavelengths. This means that a unique set of frequencies will be emitted and absorbed for each material, creating spectral bands which we can observe. By analyzing the spectra produced by known materials in laboratories here on Earth, we can determine these characteristic spectra and then compare them to stellar outputs. If a spectral feature is observed in emission, this means that the material surrounding a star is re-emitting efficiently about this frequency and is sufficiently thin that the re-emitted photons are not all reabsorbed. However, absorption features imply that the dust is geometrically and optically thick enough that the outer, cooler layers of the shell are absorbing more of the incoming photons around that wavelength.

1.3.6 Meteoritics

The second method by which we can study dust is meteoritic analysis. Most of the dust in the solar nebula was vaporized and then re-formed, losing its original isotopic signature; however,

---

[5]Meteoritic analysis will be discussed in § 1.3.6.

some grains survived and their sources can be identified. These grains can sometimes be found embedded in primitive, non-differentiated meteorites. Because meteorites were formed mostly from the same material as the Earth, we must distinguish between this (vaporized and reformed) material and the presolar grains. We can do this by noting the relative abundances of *s-process* and *r-process* elements. Examination of these mineral species and their grain morphologies can help us to determine what dust formed around previous AGB stars. Knowing the chemical composition and grain shapes which form around AGB stars allows us to predict or rule out differing scenarios for dust formation. If high abundances of *s-process* elements are found in a sample, we deduce that the sample is a remnant of AGB star outflows.

1.4 Astronomical Investigations

Dust features around cool evolved stars first began to attract attention in the late sixties, when Gillett et al. (1968) investigated deviations of stellar energy distributions from black-bodies. In the course of this study, Gillett et al. discovered a peak near 10 μm in the spectra of four late-type evolved variable stars. Woolf & Ney (1969) attributed this emission peak to circumstellar amorphous silicates. Since then there has been much interest in the nature and formation of dust grains around AGB stars.

Various attempts have been made to classify the observed dust features of oxygen-rich evolved stars (e.g. Little-Marenin & Little 1990; Sloan & Price 1995; Speck et al. 2000). All of these authors have classified the observed spectra into groups according to the shape/strength of the dust features close to 10 μm, reflecting a progression from a broad

feature to the classic narrow 10 μm feature (See Figure 1.6). This progression is expected to represent the evolution of the dust from the early forming refractory oxides (the broad feature) to the dominance of magnesium-rich silicates (the narrow 10 μm feature). An alternate explanation actually reverses this time series. In this case the condensation sequence is determined by the precise C/O ratio. Stars with a relatively low C/O ratio would exhibit strong silicate features, while stars with higher C/O ratios (but still < 1) could have spectra dominated by Al_2O_3 (alumina; Sloan & Price 1998). Another study (Egan & Sloan 2001) suggests that the geometric thickness of the dust shell can account for some of the variation in the width of the 10 μm feature; a thin shell would produce a narrower peak at this wavelength. Dijkstra et al. (2005) suggest that there is a correlation between the mass-loss rate and the shape of the 10 μm feature. Since mass-loss is expected to increase with evolution, this supports the former scenario.

1.5   Radiative Transfer Modeling

Among the tools at our disposal in the quest to determine the composition of these shells are radiative transfer modeling codes such as DUSTY (Nenkova et al. 2000), which we employed for much of the work presented here. Radiative transfer modeling works by beginning with a theoretical blackbody radiation curve and then calculating the scattering and absorption of a given distribution of grains.

DUSTY can calculate output spectra for varied stellar temperature, inner dust shell temperature (pertinent to which mineral species can form), dust density distribution, grain size distribution, optical depth, geometrical depth and dust composition/crystal structure.

Information about the composition and crystal structure can be input either in the form of n and k or as absorption and scattering cross-sections.

1.6   The 13 μm Feature

Vardya, de Jong & Willems (1986) observed 20 Mira variable stars using the Infrared Astronomy Satellite (IRAS; Neugebauer et al. 1984) Low Resolution Spectrograph (LRS). In the course of their observations, they found a previously unnoticed feature peaking between 12.5 and 13 μm. Vardya, de Jong and Willems (1986) subsequently attributed this feature to some sort of silicate. The feature was later found to be associated specifically with O-rich AGB stars (Little-Marenin & Little 1988). Further studies analyzing data from the IRAS LRS and the Infrared Space Observatory (ISO; Kessler et al. 1996) Short Wavelength Spectrometer (SWS; de Graauw et al. 1996) (SWS) (Justtanont et al. 1998; Posch et al. 1999; Fabian et al. 2001; Sloan et al. 2003) as well as ground-based spectra (Speck et al. 2000) have yielded several possible carrier species for this feature, but as of yet none has been conclusively identified.

The 13 μm feature (Figure 1.7) has several interesting characteristics which must all be accounted for and explained by any carrier candidate. First, given that it appears solely in O-rich stars, it is likely that the carrier is an oxide or silicate of some sort. It has also been observed that only about half of all oxygen-rich AGB stars possess this feature, and of those, $\sim$75-80% of semi-regular variable (SR) stars, $\sim$20-25% of Miras, and virtually no supergiants exhibit it[6] (Sloan, Levan & Little-Marenin 1996; Speck et al. 2000). As previously noted,

_____

[6]Supergiants differ from AGB stars in that they do not experience the "third dredge-up" of elements

SRs have optically thinner shells than Miras, suggesting that their shells are less dense and/or geometrically thinner. Because the 13 μm feature is associated with SR stars, this leads us to believe that either it is produced by a mineral species of low relative abundance whose spectral features are overwhelmed by those of the surrounding dust as optical depth increases, or the carrier mineral is only formed in a relatively low density environment. High density dust shells tend to promote the formation of amorphous materials as opposed to crystalline compounds because higher density implies a greater frequency of collisions between atoms and molecules. This means that atoms and molecules previously accrued by the grain have less time to migrate to the most stable locations. Therefore materials tend to clump together into amorphous or porous dust. However, recent studies of a carbon-rich star suggest that this conventional wisdom may be incorrect, with high crystallinity occurring in denser shells (see Speck et al. 2006).

Also of note is the correlation of the 13 μm feature with features at 20 and 28 μm as well as CO_2 emission lines (Begemann et al. 1997; Justtanont et al. 1998; Speck et al. 2000; Sloan et al. 2003) (See Figure 1.6). There is a possible correlation with the 10 μm feature, but this is controversial (see Begemann et al 1997; Fabian et al. 2001; Speck et al 2000; DePew et al 2006; Chapter 2). The 13 μm feature is always seen in emission and never in absorption. As radiation passes through a dust shell, it is either scattered or absorbed. If a dust grain is already hot, it will absorb visible light and re-emit at infrared wavelengths. As the radiation passes through cooler dust far from the star, dust grains absorb these infrared

---

from the helium-burning shells because they have a higher temperature and energy output. This leads to a lower internal opacity, so less convection results. This means that supergiants all remain oxygen-rich.

emissions and re-emit at even lower frequencies. Because the 13 μm feature is never seen in absorption, it has been associated with stars that possess (geometrically and/or optically) thinner dust shells. Observational studies have estimated SRs and Miras to have an optical depth $\tau = 0.05$ at $\lambda = 10$ μm (Ramdani, 2003).

With all this in mind, we attempt to constrain the 13 μm carrier species using radiative transfer modeling.
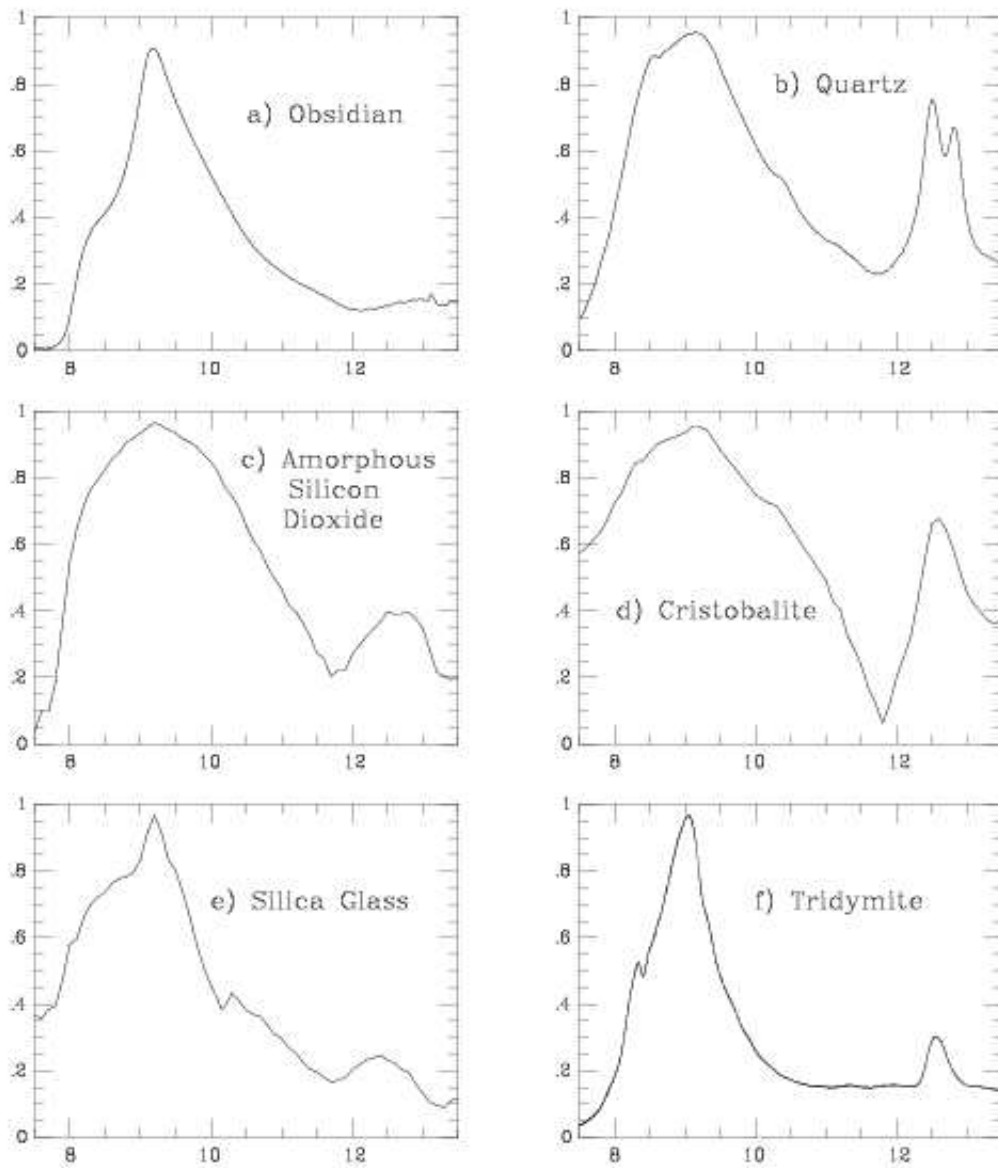
Figure 1.5: *Sample spectra of various forms of silica (SiO$_2$)from Speck (1998). The x-axis is wavelength in µm and the y-axis is the normalized extinction k.*
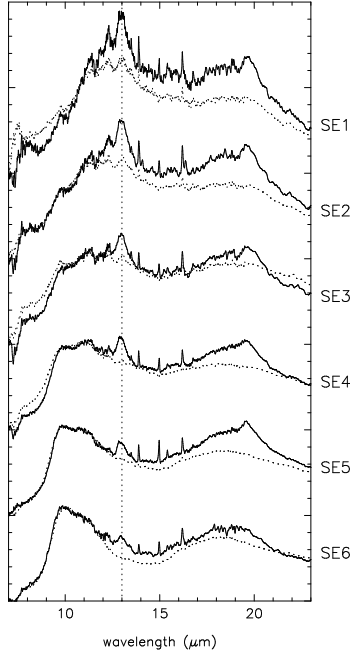
Figure 1.6: *Averaged mid-IR spectra of AGB star classes. This specific classification is based on the shape and strength of the 10 μm feature in continuum-subtracted spectra. SE stands for silicate emission. SE1 denotes the weakest 10 μm feature while SE8 has the strongest. The dotted lines indicate the averaged spectra of those stars in each SE class that do not exhibit the 13 μm feature. The solid lines indicate the averaged spectra of those stars in the same class that do exhibit it. The dotted line marks the 13 μm feature.*
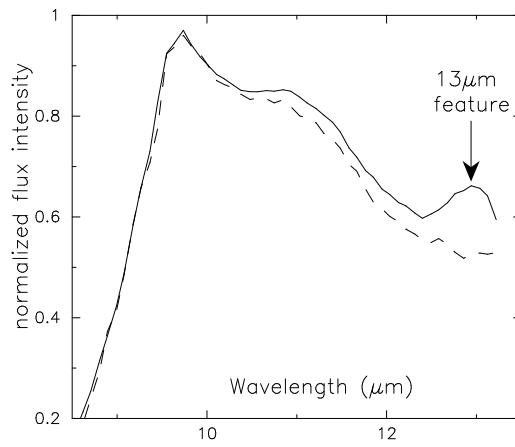
Figure 1.7: *The 13 µm feature, taken from Speck (1998). Here the average spectrum of AGB stars exhibiting the 13 µm feature is represented by the solid line. The average spectrum of those AGB stars which do not exhibit this feature is represented by the dashed line.*

Chapter 2: Corundum & Spinel

In Chapter 1, the 13 μm feature was introduced. In this chapter we investigate two of the candidate carrier minerals: corundum (α-Al$_2$O$_3$) and spinel (MgAl$_2$O$_4$).[7] As mentioned in the previous chapter, we can use meteoritic evidence to inform our conceptions of what species form around O-rich AGB stars. However, presolar meteoritic samples only preserve the hardiest grains and may not be representative of the entire range of grain shapes forming in the outflows of AGB stars. Because presolar corundum and spinel have been found in meteorites they are treated here, separately from silica. Silica has also been found in meteorites, but it is not presolar.

2.1   Meteoritic "Corundum" and Spinel

As discussed in the introductory chapter, meteoritic analysis can provide detailed information on circumstellar dust grains (see e.g. Clayton & Nittler 2004; Hoppe 2003). Al$_2$O$_3$ and spinel (MgAl$_2$O$_4$) grains have been found in meteorites (Nittler et al. 1994a,b, 1997; Huss et al. 1995) and have isotopic signatures which indicate that they were formed around oxygen-

---

[7]The contents of this chapter have been discussed in DePew et al. (2006).

rich AGB stars.[8] Thus presolar grains provide samples of circumstellar oxides that can be studied in the laboratory. Examining this presolar material can set limits on the grain size and structure of the minerals that are observed around evolved stars. Presolar Al_2O_3 grains have sizes in the range of 0.5-5 μm (Nittler et al. 1997), while the presolar spinel grains are typically smaller (0.2-0.5 μm; Zinner 2003). Only two alumina grains have been studied crystallographically (though many have been studied isotopically), one amorphous and the other crystalline[9] (Stroud, Nittler & Alexander 2004). (See § 2.2 for a discussion of the difference between crystalline versus amorphous minerals.) The crystal structure of the presolar spinel grains is not known. Clearly more crystallographic data is needed for comparison for observational evidence for these dust species. Furthermore, the scanning electron microscope (SEM) images of presolar spinel and corundum grains suggest that these grains are not spherical and not fluffy.

2.2 Effect of Grain Shape

As mentioned in Chapter 1, grain shape is very important in determining the output spectrum of a medium. In order to constrain the grain shapes which could produce the 13 μm feature, the scattering and absorption cross-sections of corundum and spinel were calculated using Mie theory for spherical grains. To calculate the cross-sections of spheroids, ellipsoids and hollow spheres, we followed the approach of Min et al. (2003). These equations follow

---

[8]While many of the published articles on Al_2O_3 grains refer to them as corundum, the majority of these have unknown crystal structures and should be referred to as alumina (Hoppe 2003).

[9]This grain should specifically be referred to as corundum; i.e. the polymorph α-Al_2O_3.

the statistical approach to calculating cross-sections (see e.g. Bohren & Huffman 1983), which assumes that a collection of irregularly shaped particles can be represented by a distribution of many simple shapes, in this case spheroids, ellipsoids and hollow spheres. The particle distributions in each of these categories are volume equivalent. Hollow spheres are used to approximate an inhomogeneous or porous medium. The typical treatment of such a situation consists of using the Maxwell-Garnett approximation (see e.g. Bohren & Huffman 1983). This approximation assumes two things: 1) the sizes of the inclusions are much smaller than the wavelength of the radiation in the host material, and 2) these inclusions are isolated so that they scatter independently. Even though these assumptions are made in the derivation of the approximation, many have found the results to be very accurate even when these conditions are not met (see e.g. Chylek et al. 2000). However, hollow spheres are used because they immediately meet both of the conditions of Maxwell-Garnett theory. Furthermore, Min et al. (2003) found that a continuous distribution of hollow spheres, although not suspected to represent the real shape of circumstellar grains, nonetheless is more successful in reproducing the observed spectra of a distribution of irregularly shaped particles than other grain shape distributions.

Figures 2.1 and 2.2 show the effects of varying the grain shape of the particles on the scattering and absorption cross-sections of corundum and spinel respectively. For spinel, both spheroidal and ellipsoidal grains cause the strength of the 13 μm feature to be reduced by about one-half relative to the spherical grain feature. Furthermore, the peak is shifted about 0.5 and 1.0 μm to 13.5 and 14.0 μm for spheroids and ellipsoids respectively. The wavelength shift for hollow spheres is even more noticeable. Here the peak is shifted almost

to 14.5 μm.
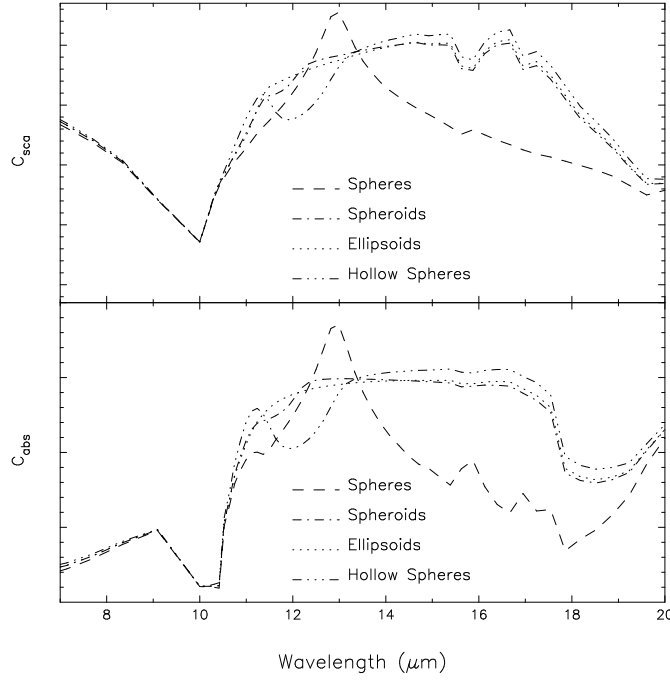
Figure 2.1: *Scattering and absorption cross-sections of corundum showing the effects of different grain shapes. The graph utilizes a logarithmic scale. Top: Scattering cross-sections in square centimeters. Bottom: Absorption cross-sections in square centimeters.*

When we change the shape of corundum grains from spherical, the 13 μm feature also exhibits a cross-section reduction of one-half with a relatively consistent 1 μm (longward) shift for all nonspherical grain shapes. Furthermore, the weak 20.5 μm feature seen in the spectrum for spherical corundum grains is shifted to $\sim$22 μm and is much stronger once the grains are assumed to be nonspherical.

It is clear from Figures 2.1 and 2.2 that if corundum or spinel were the carrier of the 13 μm feature, the grains would necessarily be spherical. If corundum or spinel were found to be present predominantly in nonspherical grains, they would not emit at 13 μm and would thus be automatically excluded from this investigation. Further meteoritic studies into the

25
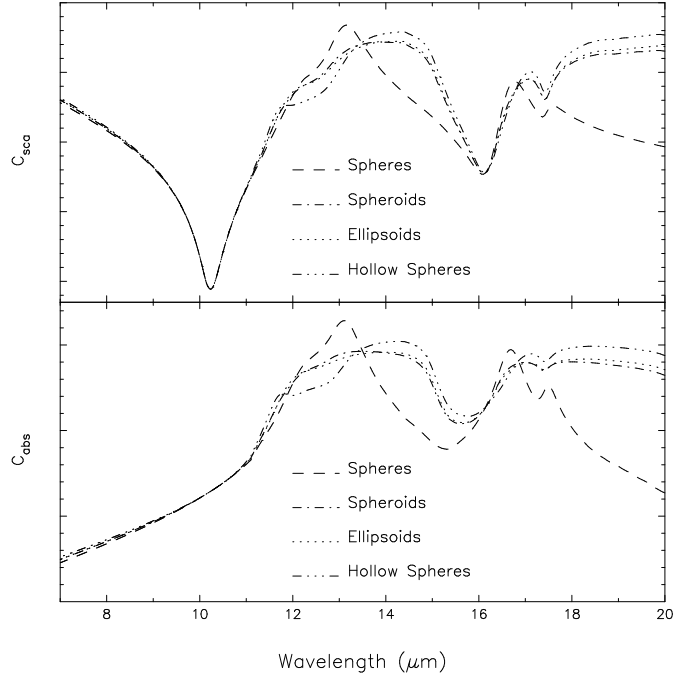
Figure 2.2: *Same as Figure 2.1, but for stoichiometric spinel.*

typical grain shape and crystal structure of these minerals in presolar grains would greatly aid us in the identification of the 13 μm carrier.

Previous IR studies of crystalline spinel have found spectral features at wavelengths longward of 13.5 μm (e.g. Chopelas & Hofmeister 1991; Hafner 1961; Preudhomme & Tarte 1971). Indeed, it was these previously published spectra that prompted Speck (1998) to ignore spinel in her discussion of mid-IR dust features because it did not appear to have any features in the 7.5-13.5 μm window and would therefore not be a candidate for the 13 μm feature. These previous studies were for terrestrial samples and imply that for naturally occurring spinel on the Earth, the grains are not spherical in shape. This begs the question, Why should circumstellar environments form only spherical oxide grains? The answer may be as simple as the difference in pressure regimes between terrestrial mineral formation and stardust formation. However, for crystalline minerals, one might expect growth to occur

according to the crystal structure, and thus similarities between terrestrial and circumstellar grain shapes may be inevitable.

It has been proposed that grain shape is dependent on the temperature of formation of the grains, with warmer dust forming spherical grains, while species formed in cooler environments tend toward spheroidal formations (Voshchinnikov & Semenov 2000). It is possible that this could explain why corundum (and/or spinel) may form only spherical grains. This also suggests that corundum (and/or spinel) formation is inhibited at low temperatures because we do not see the features associated with other grain shapes.

2.3 Radiative Transfer Modeling Parameters

We use the radiative transfer modeling code DUSTY to produce synthetic spectra of dust shells which contain corundum and spinel. Because, as noted in the previous section, only spherical grains of either mineral are capable of producing a feature at 13 μm, only spherical grains have been modeled.

DUSTY can be used to observe the effect of varying blackbody temperature of the star, optical depth of the dust shell, inner dust shell temperature, dust composition, dust density distribution and grain size distribution. In our case we fixed the blackbody temperature of the star at 3000 K and inner dust shell temperature at 800 K. Although AGB stars can range in temperature from 2500-3500 K, we do not vary the blackbody temperature or the inner dust shell temperature of the star in our models. We have found that varying the temperature of both the blackbody star temperature and the inner dust shell has little effect on the output spectrum, as illustrated in figures 2.3 and 2.4. The radial distribution of dust

is set at $\rho \propto 1/r^2$, thus assuming a constant mass-loss rate and constant wind velocity. Using this relation, IR spectra of AGB stars can be reproduced reasonably well (see e.g. Rowan-Robinson & Harris 1982). The modeling also employs the MRN grain size distribution (Mathis et al. 1977). This means that the number of grains of a certain radius a is:

$$n(a) \propto a^{-q}$$

where q is a parameter set at 3.5 and a ranges from 0.005 μm to 0.25 μm. In our models, we have varied optical depth and dust composition using optical constants n and k for corundum from Gervais (1991) and those for spinel from Fabian et al. (2001). The majority of the dust is assumed to be silicate. Variation in the composition of the dust is studied by changing the oxide to silicate mass ratios. We also investigate the effect of including amorphous alumina in the dust. Optical constants for warm silicates and amorphous alumina were drawn from Ossenkopf et al. (1992) and Begemann et al. (1997) respectively.

2.4 Corundum

Figure 2.5 shows the model spectra for mixtures of corundum and warm silicates, with the optical depth held constant at $\tau_{10\mu m}{=}0.05$ in accordance with Ramdani's optical depth estimate for SRs and Miras. As the relative abundance of corundum is reduced, the 13 μm feature of corundum is seen to gradually decrease in prominence until at 5% percent corundum and 95% warm silicates, the height of the feature is such that the 13/9.7 μm flux ratio appears similar to that observed in AGB stars exhibiting the feature. Since only 1% of the dust needs to be corundum in order for its 13 μm feature to be observable, our models
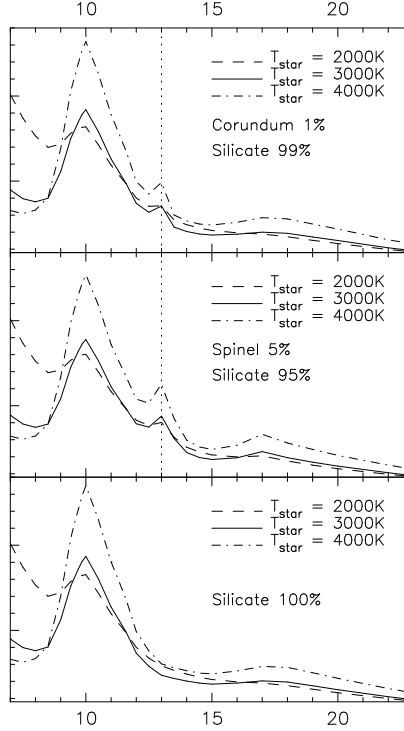
Figure 2.3: *Effect of stellar temperature on the shape, position, and relative strengths of IR dust features: Top: 1% corundum, 99% warm silicate; Middle: 5% spinel, 95% warm silicate; Bottom: 100% warm silicate. The dotted line indicates the location of the peak of the 13 μm feature.*

suggest that if corundum forms, it will be seen. One of the objections to the attribution of the 13 μm feature to corundum is that it should be accompanied by a weaker feature at ~20.5 μm that is not seen in observed spectra (Begemann et al. 1997). However, the 20.5 μm feature is intrinsically weak, and it has been suggested that this feature would be difficult to observe (Glaccum 1995). This is supported by our models which show that, at low relative abundances, the corundum ~20.5 μm feature cannot be seen, being well hidden by the silicate features. Figure 2.5 shows that the 20.5 μm feature does not appear until the relative abundance of corundum exceeds ~25%. Therefore, we should not rule out corundum
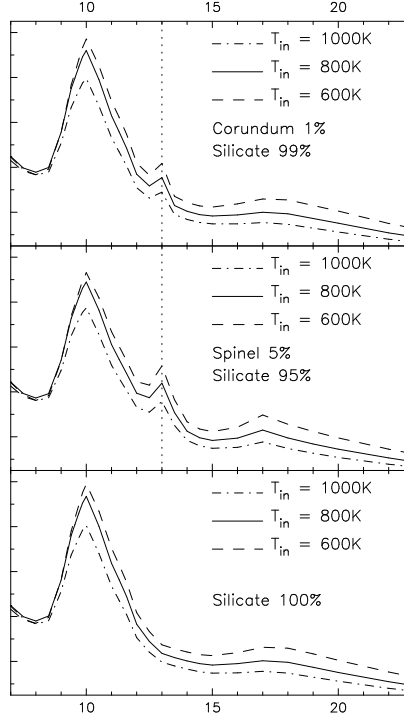
Figure 2.4: *Same as Fig. 2.3, but for the effect of dust condensation temperature (i.e., dust temperature at the inner radius of the circumstellar shell).*

as the carrier of the 13 μm feature on these grounds.

Since a dust composition of 99:1 silicate to corundum yields a promising spectrum at $\tau_{10\mu m} = 0.05$, we have investigated the effect of optical depth variations on the emerging spectra. At low optical depths ($\tau_{10\mu m} = 0.05$, 0.1, and 1), the 13 μm feature is visible and at a reasonable intensity (Fig. 2.6). However, at $\tau_{10\mu m} = 5$, the feature goes into absorption. This happens at lower optical depths for higher relative abundances of corundum. The 13 μm feature has never been observed in absorption, limiting the $\tau_{10\mu m}$ versus relative abundance space in the stars that exhibit this feature. Furthermore, this feature is not seen in O-rich evolved stars with very high optical depths (Maldoni et al. 2005), suggesting that high densities may preclude the formation of corundum (if the 13 μm feature is indeed
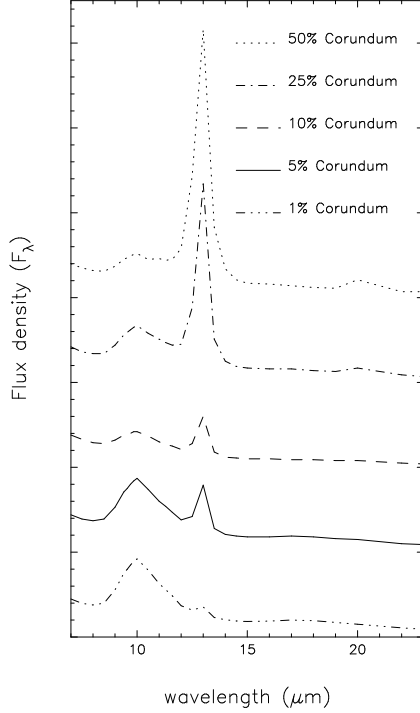
Figure 2.5: *Model 7-23 μm spectra for different mixtures of corundum and warm silicates at fixed optical depth ($\tau_{10\mu m} = 0.05$). In each case the dust composition is given by the percentage of corundum, with the remainder of the dust comprised of warm silicates only.*

attributable to corundum).

2.5 Spinel

In Figure 2.7, we present the spectra from the spinel models of various relative abundances, again at $\tau_{10\mu m} = 0.05$. From this we can see that, in order for the 13 μm feature to appear with the observed strength, it would be necessary to set spinel at $\gtrsim 5\%$ of the dust composition, with warm silicates comprising the remainder. At this relative abundance, there is a clearly observable 17 μm feature. Both Sloan et al. (2003) and Heras & Hony (2005) have shown that this feature does not occur in the *ISO* spectra of AGB stars that exhibit the 13 μm
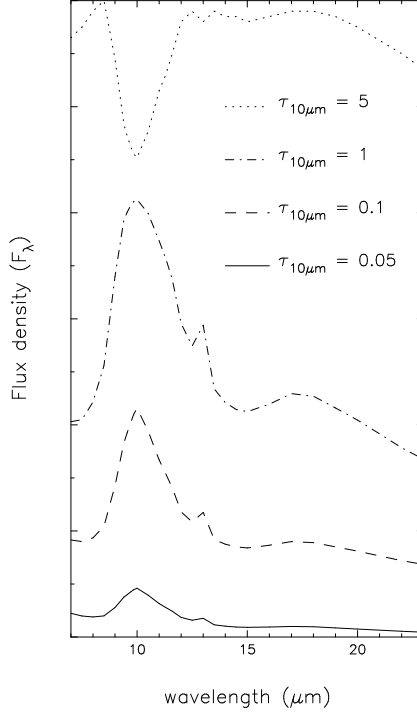
Figure 2.6: *Model 7-23 μm spectra for a fixed mixture of corundum (1%) and warm silicates (99%) at different optical depths.*

feature.

Figure 2.8 shows the effect of optical depth on the spinel 13 μm feature. In these models the relative abundances are 5% spinel and 95% silicate. In all cases, the models predict a small but noticeable emission feature at 17 μm. Note that this feature is seen in emission even at high optical depth, when the silicate feature is seen in absorption. While Posch et al. (1999) suggest that there is a 17 μm feature in their objects' spectra, the observed feature has an FWHM of only 0.15 μm (Sloan et al. 2003), much narrower than the model data for the spinel feature. The DUSTY models for spinel grains confirm this (Fig. 2.9. The lack of observed 17 μm features rules out spinel as the carrier of the 13 μm feature.
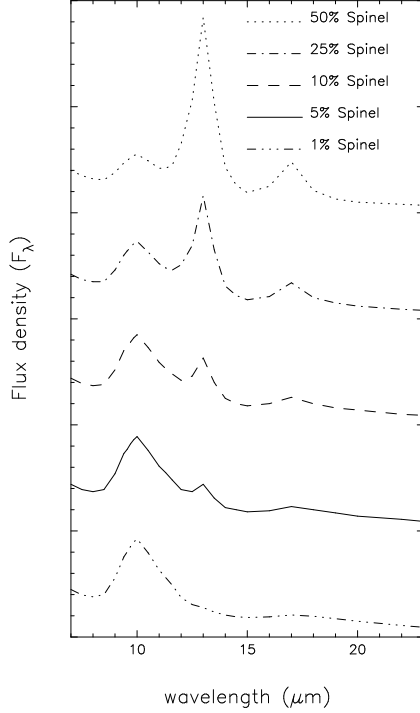
Figure 2.7: *Model 7-23 μm spectra for different mixtures of spinel and warm silicates at fixed optical depth ($\tau_{10\mu m}$= 0.05). In each case the dust composition is given by the percentage of spinel, with the remainder of the dust comprised of warm silicates only.*

2.6 Amorphous Alumina

Lower number silicate emission classes (see § 2.7 below) are believed to have a significant spectral contribution from amorphous alumina (as opposed to silicate domination for the higher SE classes), which leads to the broad feature at ~10 μm (see e.g. Speck et al. 2000). Therefore, it is possible that amorphous alumina serves to mask the presence of other less abundant mineral species in the dust shell. For this reason, amorphous alumina has been incorporated into the models to see how its presence would change observational spectra. As Figure 2.10 shows, the 13 μm feature is present in all classes, but the broad 10 μm feature, associated with amorphous alumina, does not seem to hide it.
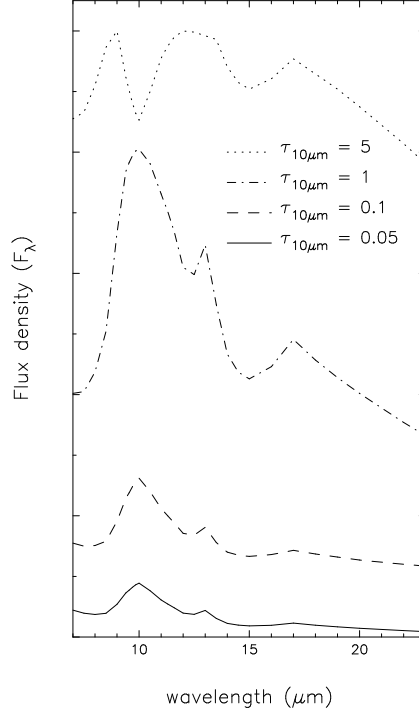
Figure 2.8: *Model 7-23 μm spectra for a fixed mixture of spinel (5%) and warm silicates (95%) at different optical depths.*

Figure 2.11 shows the models in which the dust composition comprises only corundum and amorphous alumina. Even at very low relative abundances (1% corundum, 99% alumina), the corundum 13 μm feature is easily seen. Figure 2.12 shows the effect of optical depth on these models and demonstrates that the corundum feature is seen at most optical depths. This shows that the introduction of amorphous alumina grains cannot mask the corundum 13 μm feature unless the optical depth is very high. If corundum is present, it will be observable.
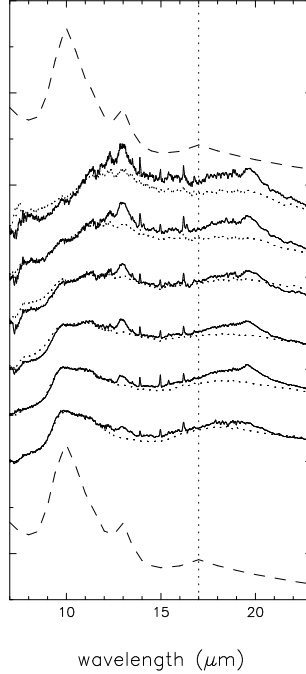
Figure 2.9: *Comparison of the 5% spinel mixture at $\tau_{10\mu m}= 0.05$ with spectra from stars of different silicate emission indices. The 17 μm feature is marked for clarity.*

2.7 Comparison with ISO SWS Spectra

The Infrared Space Observatory (*ISO*) was an astronomical satellite that was operational between the years of 1995 and 1998, taking observations in the infrared region of the spectrum (Kessler 1996). On board *ISO* were four instruments, among them the Short-Wave Spectrometer (SWS), which took data in the 2.4 to 45 μm band.

By using the spectral classification system developed by Sloan & Price (1995, 1998), Sloan et al. (2003) reinvestigated the observed 13 μm feature using *ISO* SWS observations. Their spectral classification uses the shape/strength of the silicate feature to divide observed spectra into eight categories (designated by SE#, where # = 1-8; SE8 has the strongest classic silicate feature, SE1 the weakest). Figure 2.10 compares the continuum-subtracted average spectra for each silicate class (see also Fig. 1 of Sloan et al. 2003) with the spectra

35
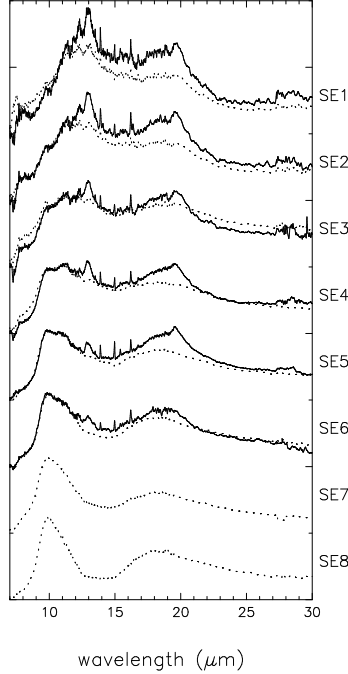
Figure 2.10: *Continuum-subtracted ISO SWS spectra of O-rich AGB stars that do (solid line) or do not (dotted line) exhibit the 13 μm feature. For a description of the SE classes, please see Sloan & Price (1995, 1998), and Sloan et al. (2003).*

exhibiting the 13 μm feature separated from those that do not. This figure suggests that the 13 μm feature is strongest in the SE1 class and weakens with increasing SE number. However, as shown in Figure 2.13, the 9.7/13 μm ratio shows an almost identical trend for the spectra without the 13 μm feature, suggesting that the apparent strengthening of the 13 μm feature is an artifact of the increasing underlying dust emission at this wavelength (probably due to amorphous alumina). It is assumed that the only difference between the circumstellar shells that exhibit the 13 μm feature and those that do not is that one has an extra component giving rise to the 13 μm (and associated) features. By dividing the spectrum with the feature by the spectrum without for each of the SE classes, we find that the residual spectrum remains approximately constant (see Fig. 2.14). The strength of the

36
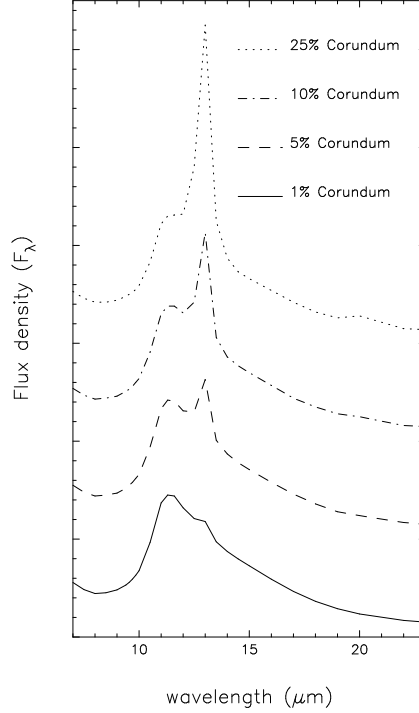
Figure 2.11: *Model 7-23 μm spectra of different mixtures of corundum and amorphous alumina at fixed optical depth ($\tau_{10\mu m}$ = 0.05). In each case the dust composition is given by the percentage of corundum, with the remainder of the dust comprised of amorphous alumina only ($\tau_{10\mu m}$ = 0.05).*

extra 13 μm emission does not change with the SE class. This implies that the relative abundance of the 13 μm carrier remains more or less constant, regardless of the trends in the other spectral features. Figures 2.15, 2.16 and 2.17 show how the models compare to the observations presented in Sloan et al. (2003). For classes SE1 and SE2 the relative abundance of corundum needed to match the strength of the observed 13 μm feature is ∼5%-10%. While the 10 μm silicate feature in these classes is weak, it is still clearly present. Amorphous alumina is also necessary to match the shape of the spectrum between 10 and 12 μm. Classes SE3 and SE4 show a similar structure, with a corundum relative abundance

37
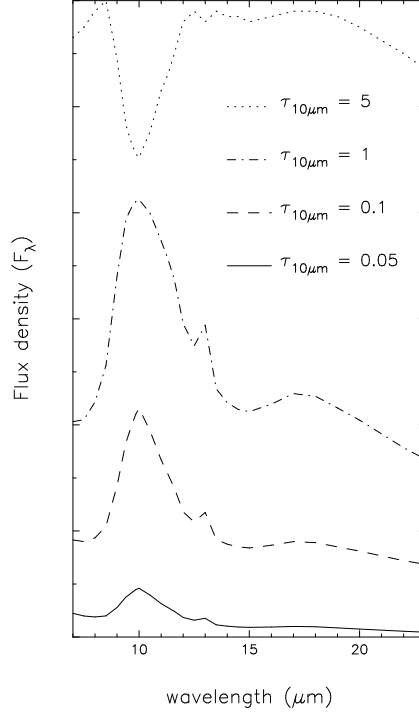
Figure 2.12: *Model 7-23 μm spectra for a fixed mixture of corundum (1%) and amorphous alumina (99%) at various optical depths.*

in the ∼5%-10% range and contributions from both silicates and amorphous alumina. The silicate contribution is stronger than for classes SE1 and SE2 while the contribution of alumina is weaker. For classes SE5 and SE6, the silicate contribution is much stronger. The alumina contribution is greatly weakened, but some amorphous alumina is still needed to match the shape of the spectrum between 10 and 12 μm. The 13 μm feature now requires ∼5% corundum. These models show that the spectra of all 13 μm objects are consistent with a relative abundance of corundum of approximately 5%. In all classes (SE1-SE6), the shape of the spectrum between ∼8 and ∼12 μm can be explained by differing relative abundances of silicate and amorphous alumina.

The most obvious failure of these models is in fitting the 16-22 μm region. The models
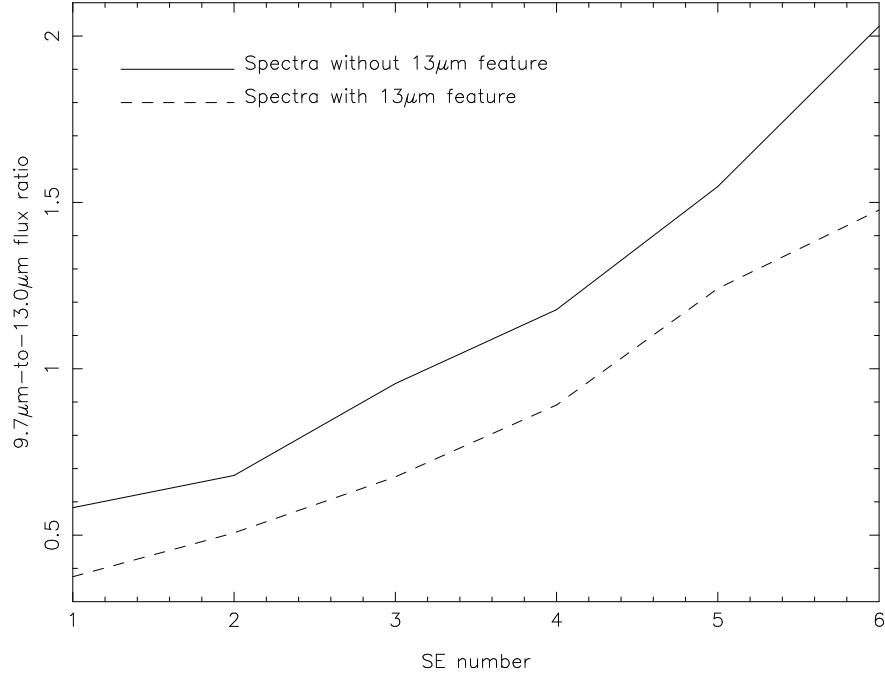
Figure 2.13: *Ratios of the 9.7 and 13 µm fluxes as a function of silicate emission index among spectra with (solid line) and without (dashed line) the 13 µm feature.*

are not able to account for the strong, broad feature in this region. Even models with a large amount of silicate cannot reproduce this feature.

2.8 Conclusions

Using DUSTY, it has been shown that spinel is unlikely to be the carrier of the 13 µm feature. Its 17 µm feature is too broad to fit observational spectra of AGB stars exhibiting the 13 µm feature (Fig. 2.9). The narrow observed 17 µm feature is probably produced by CO_2 (Sloan et al. 2003) or some other gaseous component.

Our models suggest that if corundum is present in an AGB dust shell, even at very small relative abundances, it should be observable. The principal argument against corundum was the lack of observation of its 20.5 µm feature (Begemann et al. 1997). At low relative
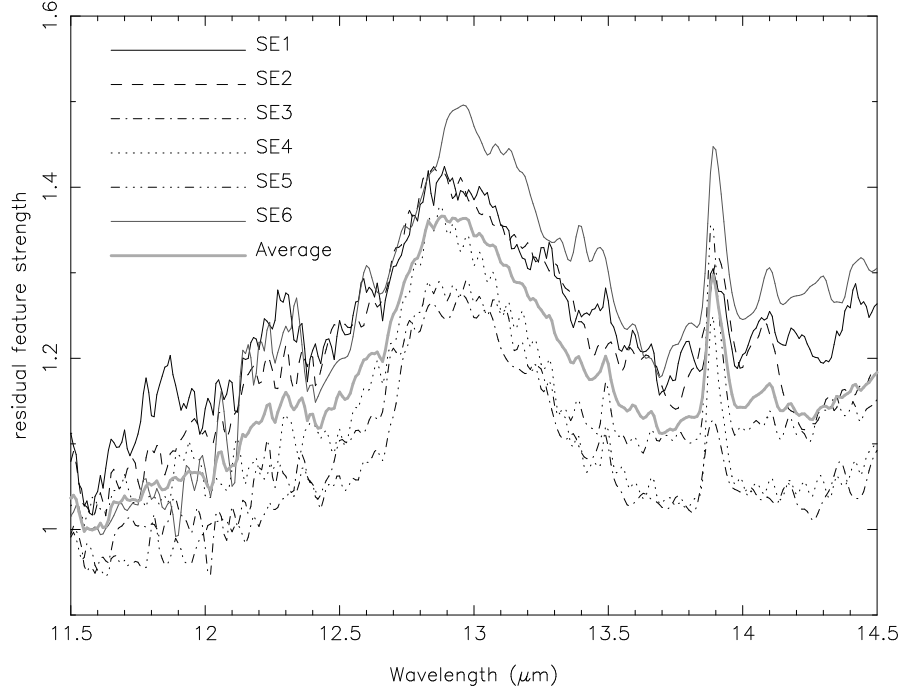
Figure 2.14: *Residual spectra. For each silicate emission index, the average spectrum that exhibits the 13 μm feature has been divided by the average spectrum that does not show this feature.*
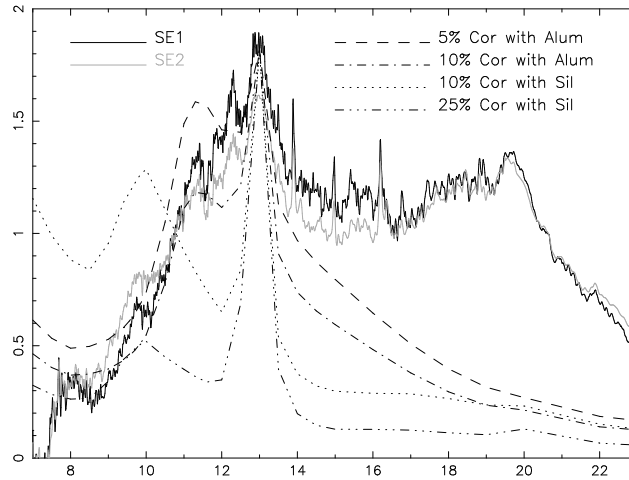
Figure 2.15: *Comparison of the corundum models with the continuum-subtracted spectra from stars the SE1 and SE2 classes. For a description of the SE classes, please see §4.4, Sloan & Price (1995, 1998).*
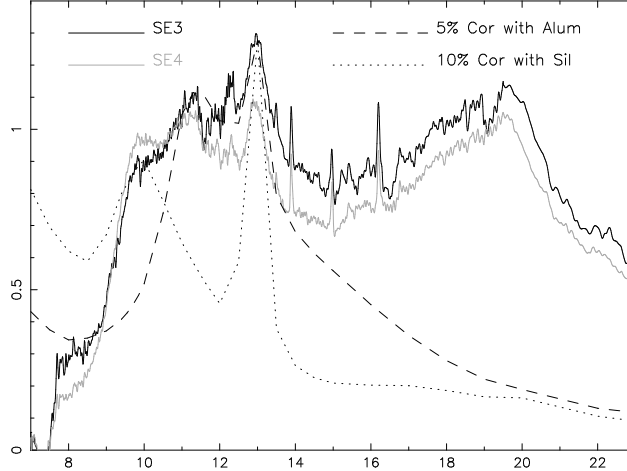
Figure 2.16: *Comparison of the corundum models with the continuum-subtracted spectra from stars of the SE3 and SE4 classes.*
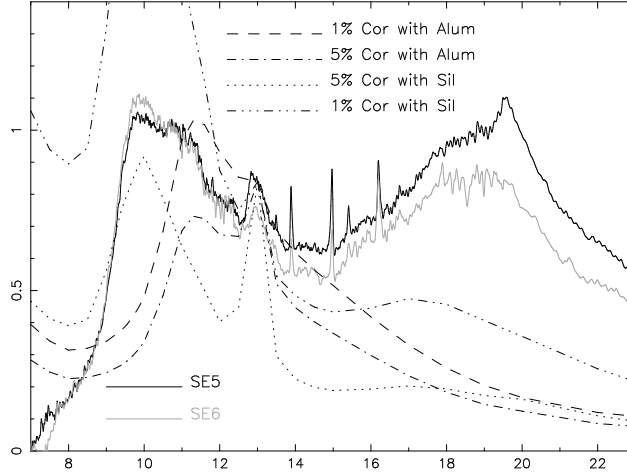
Figure 2.17: *Comparison of the corundum models with the continuum-subtracted spectra from stars of the SE5 and SE6 classes.*

abundances (1% corundum), the 13 μm feature is clearly visible, but the weak 20.5 μm feature is not seen, being effectively hidden by the broad amorphous silicate emission. It is clear from these models that the 20.5 μm feature should not be used to determine the presence or absence of corundum in AGB stars. Corundum is still a viable carrier for the 13 μm feature. Our models suggest that, if corundum is indeed the carrier of the 13 μm

feature, it is present at a relative abundance of ∼5% for all stars that exhibit the feature.

The 13 μm feature is associated predominantly with semiregular variable stars. If corundum is the carrier of the 13 μm feature, we must account for its appearance in many SRs and few Mira variables. Since Mira variables are expected to have higher mass-loss rates, the density of the dust forming region in Mira variables will be higher than in SRs. These high densities may preclude the formation of corundum, instead forming amorphous alumina. However, the models shown in Figure 2.15 suggest that there is always some amorphous alumina present in these dust shells. The shape of the 10 μm feature in the SE classes is a combination of silicate and amorphous alumina (see also Speck et al. 2000). The occurrence and strength of the 13 μm feature do not correlate with the relative abundance of amorphous alumina. If high densities cause Al_2O_3 to form amorphous rather than crystalline grains, there should be an anticorrelation between the strength of the amorphous alumina feature and that of corundum. As shown in § 2.7, the strength of the 13 μm feature is remarkably constant across all SE classes. Under these circumstances, it is difficult to understand what causes the corundum to be associated with SRs and not with Mira variables. Our models show that even low relative abundances of corundum will give rise to an observable 13 μm feature, so simply making more silicate and/or amorphous alumina will not hide the feature. It is possible that the corundum grains are more effectively coated by silicates in Mira variables, but this must also happen to some extent in SRs, as we expect Al_2O_3 grains to act as seed nuclei for silicate formation (e.g. Salpeter 1974).

The aim of the models presented here is to understand the 13 μm feature; consequently, some other features are not well fitted by our models. In particular, the models presented in
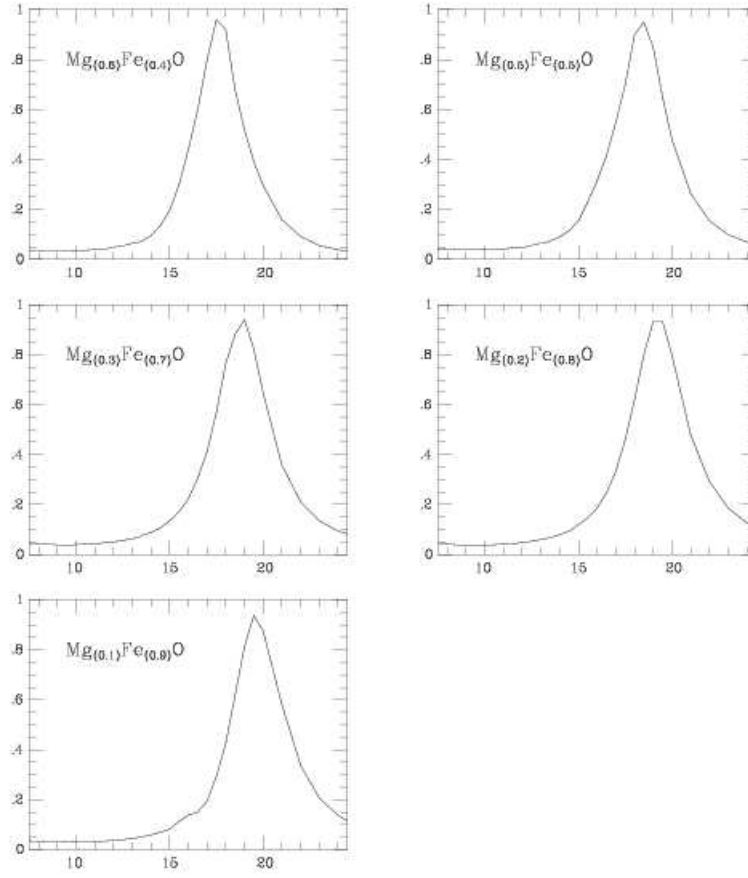
Figure 2.18: *Laboratory spectra of magnesium iron oxides from Speck (1998). The x-axis is wavelength in μm while the y-axis is the normalized extinction coefficient k.*

§ 2.4 fail to fit the strong, broad feature in the 16-22 μm region. Even models with a large amount of silicate cannot reproduce this feature. It is possible that the emission in the 16-22 μm range is produced by other oxides, i.e. MgO-FeO. These minerals would be expected

to form as a by-product of the formation of silica (SiO_2). The silicates that dominate the spectra of many O-rich AGB stars basically form by reacting SiO_2 with MgO and FeO (e.g. Rietmeijer et al. 1999; Lodders & Fegley 1999). If the reactions reach equilibrium, all these oxides become incorporated into silicates, and there should not be spectral features associated with MgO-FeO (see spectra in Figure 2.18) or SiO_2. However, if equilibrium is not reached, which may be possible in the less dense SR dust shells, we might expect to have residual SiO_2, MgO and FeO grains in these circumstellar dust envelopes contributing to the spectrum. These metal oxides form a compositional series of the form $Mg_xFe_{(1-x)}O$ ($0 \leq x \leq 1$). There are spectral features associated with these minerals that occur in the range $\sim$15-25 μm (Henning et al. 1995; Begemann et al. 1995; Hofmeister et al. 2003), with the pure MgO endmember peaking at approximately 25 μm and the pure FeO endmember peaking at approximately 20.5 μm. The intermediate compositions are reported to have features in the $\sim$15-20 μm range (Begemann et al. 1995). If the strong broad feature(s) seen in the 16-22 μm range is (are) produced by the MgO-FeO minerals, we would also expect to see SiO_2 features, which could potentially explain both the 13 μm feature (and remove the need for corundum grains), and the $\sim$10 μm feature, currently attributed to silicates. Silica may also be responsible for the 28 μm feature discussed by Sloan et al. (2003), as the optical constants of quartz (a polymorph of SiO_2) show that there should be an emission feature close to this wavelength (Spitzer & Kleinman 1961). Detailed modeling and discussion of the silica hypothesis will appear in Chapter 3.

Chapter 3: Silica

In this chapter silica (SiO_2) is discussed. As mentioned in the previous chapter, no presolar silica has yet been found in meteoritic samples. There is a noted dearth of circumstellar silicate specimens in meteorites, despite their high cosmic abundance (Messenger & Bernatowicz, 2000; Alexander et al. 2001). One possibility is that silicates were more prone to destruction by parent-body or nebular processing in the early solar system (Messenger et al. 2003). It is possible that presolar silica, like the silicates to which it is chemically related, is also destroyed in these same processes. Presolar silicates are difficult to find because chemical solutions may be used to dissolve the surrounding meteoritic material when searching for C-rich grains and Al-rich oxides; because presolar silicates are chemically identical to silicates that formed within the solar nebula, isotopic studies must be done in situ (Clayton & Nittler 2004).

3.1 Polymorphs

Silica can take on several crystal structures in low pressure regions: α-quartz, β-quartz, tridymite and crystobalite. There are two other recognized polymorphs, coesite and stishovite, but these are unlikely to be found in circumstellar dust shells because they form at pressures

of $\gtrsim 20$ kilobars, far above the near-vacuum around AGB stars.

Silica may also take on amorphous structures in the form of glasses such as lechatelierite. It is possible that these amorphous materials could also produce a 13 μm feature (See Figure 3.1).

3.1.1   Quartz

Quartz is the only silica polymorph that is stable at Earth surface temperatures and pressures. Quartz can be divided into α-quartz, with rhombohedral crystal structure, and β-quartz which is hexagonal. α-quartz forms at temperatures $<$ 846 K at 1 atm, while β-quartz will form between 846 and 1140 K at the same pressure. The two are very similar in structure and refractive indices, so they are here collectively referred to as quartz.

The optical constants for quartz were taken from Spitzer & Kleinman (1961).

3.1.2   Tridymite and Cristobalite

Tridymite forms at temperatures of 1143-1743 K at Earth surface pressures, above the formation temperature of quartz and below that of cristobalite, but formation temperatures can be altered when pressure is varied (Lodders & Fegley 1999). Like β-quartz, tridymite exhibits a hexagonal crystal structure. Though Rietmeijer et al. (1999) found a small number of spherical tridymite grains in an experimental gas-to-solid condensation of a Mg-Fe-SiO-H_2-O_2 vapor, tridymite is thought by many mineralogists to require a flux or mineralizer,[10] such as water, for its formation and to not be a stable state of silica (see e.g. Stevens et al.

---

[10] A mineralizer is defined as an element which combines with a metal to form an ore.
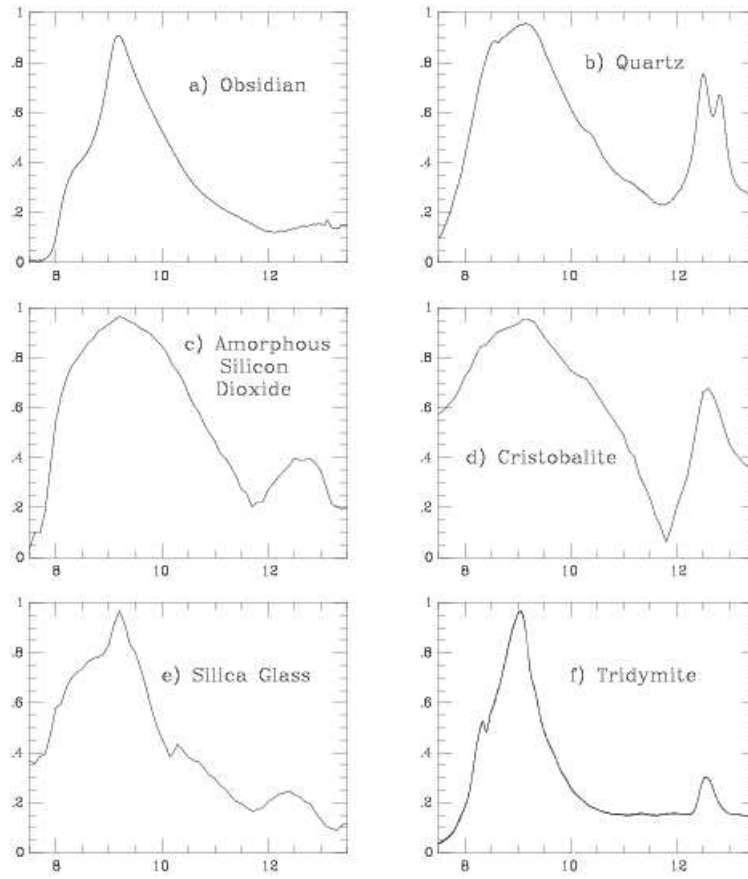
Figure 3.1: *Laboratory spectra of different polytypes and glasses of silica. Obsidian is not pure silica, but rather contains large amounts of iron, magnesium and other elements. It is formed when volcanic lava is cooled through contact with water. Silica glass results when the silica is rapidly cooled, differentiating it from the amorphous silicon dioxide above it. The other three spectra are from silica polytypes discussed in this chapter.*

47

1997). Considering the low density of matter in environments typical of circumstellar dust shells, it may be improbable to find tridymite.

Cristobalite, which forms cubic crystal lattices, is only metastable[11] at the temperatures and pressures assumed to dominate in the circumstellar dust shells. It is only stable when it forms at temperatures between 1470 and 1986 K (at 1 atm). However, once formed it can persist indefinitely; i.e. it will not transform into quartz on cooling.

3.1.3 Crystal Structure

As discussed in Chapter 1, spectroscopy can be used to identify dust components by comparing observed spectra to those in the lab for various minerals. Crystal structure can affect the relative strengths and positions of the spectral features. For the purpose of comparing spectral features, Figure 3.2 shows the Q_{abs} of quartz with the absorbances[12] of tridymite and cristobalite. Note how while all three polymorphs exhibit a 9 and a 13 μm feature, cristobalite also possesses a large, wide feature at 20 μm much larger than its own 13 μm feature. Cristobalite also shows a 16 μm feature that the other two polymorphs do not exhibit, as well as a 26 μm feature and a small bump at 8.3 μm. Tridymite has a broad feature between 13 and 17 μm and a peak at 20.8 μm. Quartz shows a feature between 18 and 22 μm that appears to be of the same relative intensity as its feature at 12.5-13 μm. It also possesses a small feature at 14 μm.

---

[11] A metastable state is a transient and unstable state that is nonetheless relatively long-lived.

[12] Absorbance is proportional to Q_{abs}. These two quantities only differ by a scaling factor.
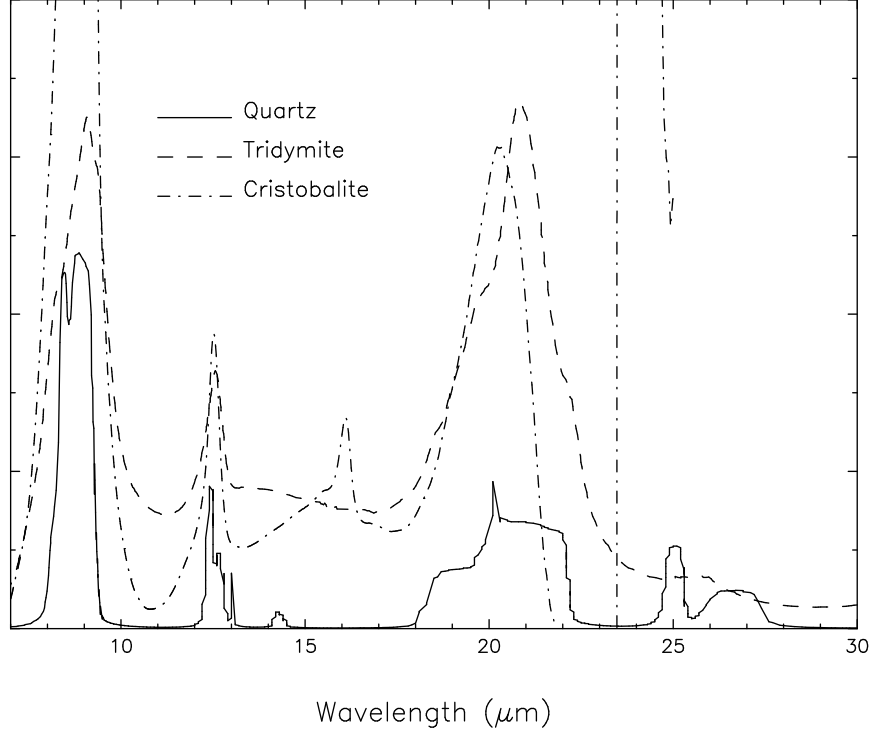
Figure 3.2: *The Q_{abs} factors for quartz contrasted with the absorbances of tridymite and cristobalite.*

3.2 Grain Shape Effects

Because we only possess optical constants n and k for quartz, we have limited our study of different grain shapes to this polymorph, but we hope to extrapolate the trends for the others. In Figures 3.4 and 3.3, we can see how the grain shape alters the absorption cross-section. Note that all features but the 13 μm feature are shifted to longer wavelengths with non-spherical grains. In the course of our modeling, we employed spheroidal grains when looking at non-spherical grains in general because all non-spherical grains exhibit very similar cross-sections. It should also be noted that the 9 μm feature of quartz is much less prominent in non-spherical grains than in spherical grains.

It is also noteworthy that the 26 μm feature of spherical grains can be shifted to 27

49

μm with spheroidal grains. This is significant because Sloan et al. (2003) found a strong correlation between a 28 μm feature and that at 13 μm in astronomical spectra. It may be possible that grain size and crystal structure might cause this 27 μm peak to be shifted to an even longer wavelength.

In order to model silica grains, we took the scattering and absorption cross-sections of quartz along both the parallel and perpendicular polarization axes of a crystal. The parallel and perpendicular axes each have their own set of optical constants. Therefore we assumed a distribution of silica grains, one-third of them situated such that the observer's line of sight is along the parallel axis and one-third aligned along each of the two perpendicular axes. Figures 3.3 and 3.4 show the absorption cross-sections along the parallel and perpendicular axes respectively. To do this, we multiplied the scattering and absorption cross-sections by one-third for the parallel axis and those for the perpendicular axis by two-thirds, then added these two quantities together. It was also necessary to model just one grain size at a time, as discussed below.

3.3   Model Input Parameters

3.3.1   Grain Shape

To do our models we used spheroidal grain cross-sections. As noted before, grain shape can shift spectral features of silica to longer wavelengths. (See Figure 3.5 for comparison of spherical and non-spherical grain shapes.) We also employed the cross-sections of one grain size at a time. See Figure 3.6 for the comparison between three models with different grain
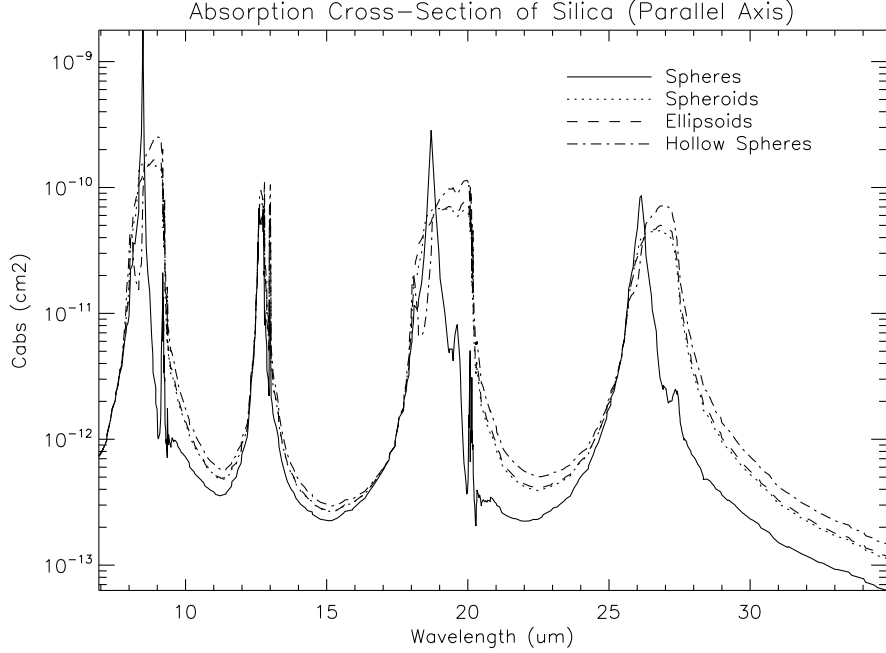
Figure 3.3: *The absorption cross-sections of quartz along the parallel (ordinary) axis.*

sizes. There is little difference in the modeled output of different grain sizes. Except for the fact that 1 μm grains cause the 9 μm feature to go into absorption at $\tau_{10\mu m}$=0.5, the only difference is in the intensity of the features. All features retain their relative intensities with the exception just noted. Thus it is reasonable to use single grain sizes.

3.3.2 Stellar and Dust Temperatures

As in our previous modeling study involving corundum and spinel (see Chapter 2), the blackbody temperature of the star was set at 3000 K. There seems to be no firm consensus on what should be the "proper" inner dust shell temperature, so it is possible that any of the three aforementioned silica polymorphs could form in these environments. Though 800-1000 K is thought to be a good approximation of this variable, this is based on the assumption that
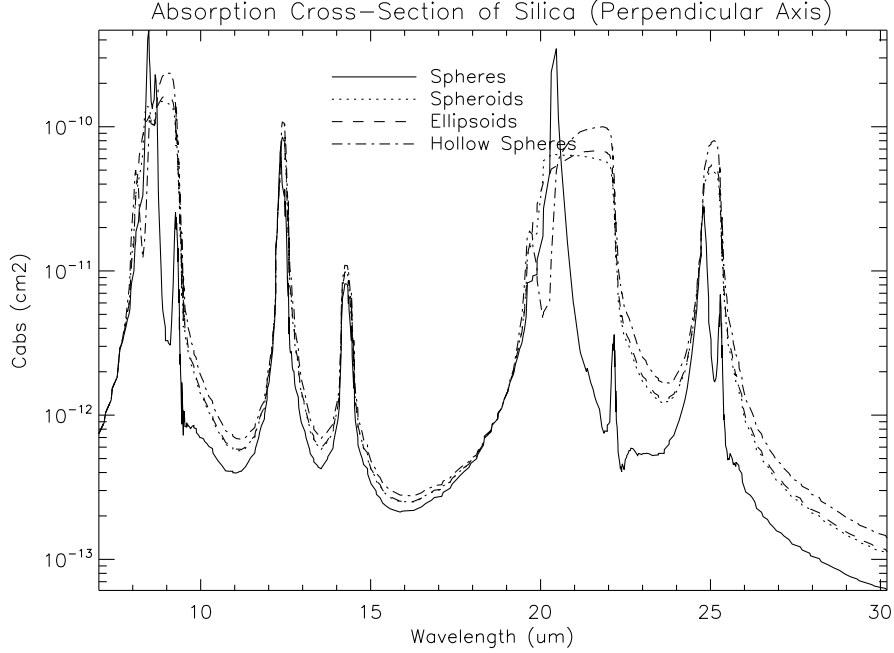
Figure 3.4: *The absorption cross-sections of quartz along the perpendicular (extraordinary) axes.*

the dust formed is amorphous silicate. Crystalline silicate can form at higher temperatures. We model the effects of a range of high (1000-2000 K) dust temperatures in Figure 3.7. For all temperatures, the 13 and 26 μm features remain visible. The primary difference is in the prominence of the 8.5 and 10 μm features. If optical depths are sufficiently high, then these features are diminished at greater temperatures. Around 2000 K the 10 μm feature goes into absorption. However, because amorphous silicates are associated with the 10 μm feature, a formation temperature of 2000 K would probably be unrealistic. We cannot model different grains in different zones with DUSTY; the grains must be co-spatial.

Justtanont et al. (1998) showed that CO_2 emission lines are well-correlated with the 13 μm feature, implying that the carrier might form in the same region as CO_2. This would

52
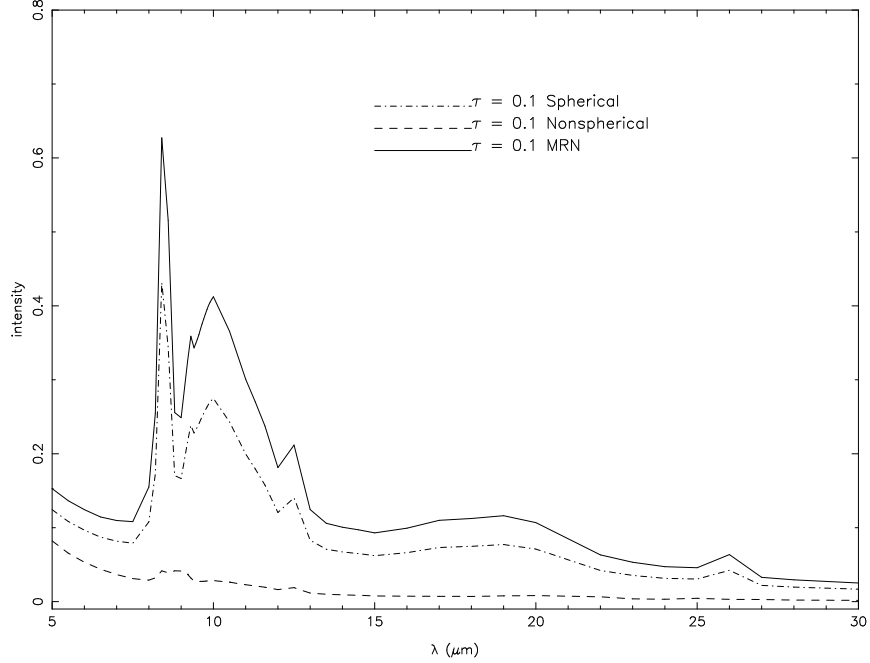
Figure 3.5: *Modeled spectra for 20% silica mixtures. Spherical and non-spherical single grain spectra are shown alongside MRN grain size distributions (spherical). Optical depth $\tau_{10\mu m} = 0.1$ and 1.*

suggest a formation temperature between $\sim$650 K and 1250 K. However, it is not known whether the carrier of the 13 μm feature is co-spatial with the CO_2. Justtanont et al. (1998) also found that stars with substantial mass-loss ($M_\odot \geq 10^{-5}$ $M_\odot$/yr) exhibited neither the 13 μm feature nor the CO_2 emission lines, but their 10 μm feature increased in intensity. This suggests that either the increased mass loss stimulates the formation of silicate dust or else prevents the formation and/or emission of 13 μm dust and CO_2 gas. Cami et al. (1998) also found the excitation temperature of this CO_2 to be $\sim$700 K, in agreement with the range suggested by Justtanont. Further observations are required to determine if the CO_2 and 13 μm features are indeed co-spatial. Such an observation would constrain the formation /excitation temperature of the carrier of the 13 μm feature.
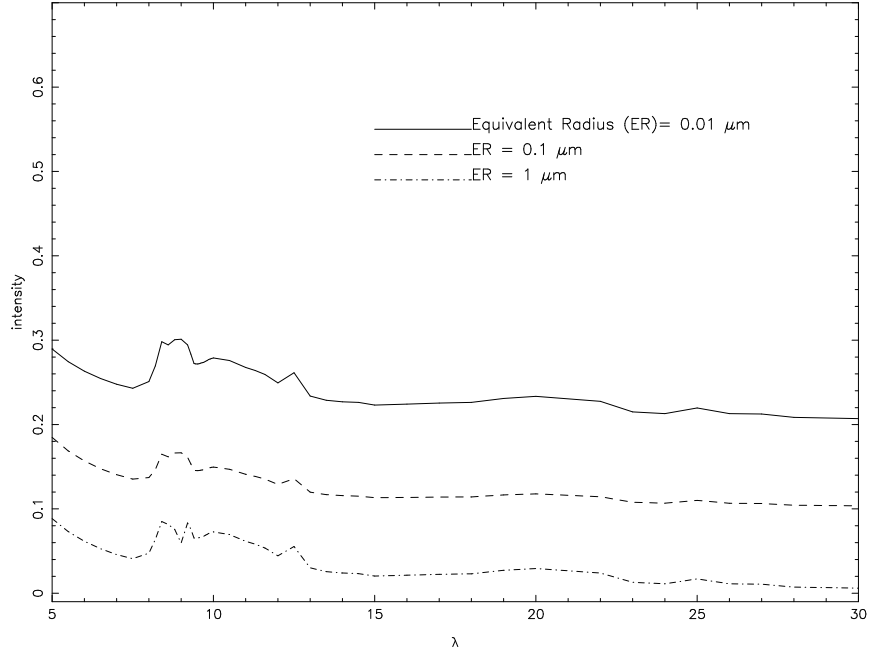
Figure 3.6: *Comparison of non-spherical grain models. The grains have 0.01, 0.1 and 1 μm equivalent radii of an equivalent volume sphere. The optical depth is set at $\tau_{10\mu m}$= 0.5 and the dust shells modeled are 20% silica.*

During our study of silica, several models of quartz-warm silicate combinations at various optical depths, relative abundances and density distributions have been produced. A continuous distribution of spheroids was used, since all non-spherical grain shapes previously studied have very similar spectra (see § 3.3.1). This spheroidal distribution is important because most presolar dust grains so far observed are non-spherical (Warren et al. 1994).

As with corundum and spinel, the effects of varying relative abundance (20%, 40%, 60% and 80% silica by mass with warm silicates comprising the remainder), optical depth and grain shape have been investigated. In addition, the effects of dust density distributions and grain size were examined. For grain size, the radius of an equivalent volume sphere is set at r=0.1 μm (as was used for corundum and spinel), 0.01 and 1 μm. This means that each

54
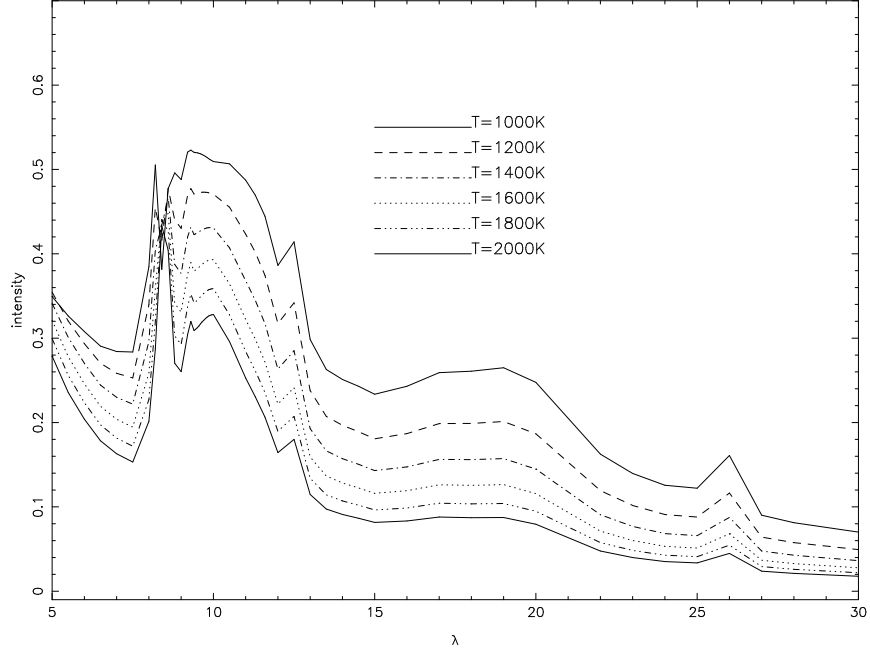
Figure 3.7: *Comparison of spherical MRN grain distributions at varying inner dust shell temperatures. The dust shell models are 20% silica and the optical depth $\tau_{10\mu m} = 0.5$.*

grain occupied the same volume as would a sphere of radius r. In each model, only one grain size was used. For our silica models, unless otherwise noted, the cross-sections of spheroidal grains are employed.

We also consider the effect of the relative thickness of the dust shell. This variable is equal to R_{out}/R_{in} where R_{out} is the outer radius of the dust shell and R_{in} is the inner radius. A geometrically thin shell indicates either short-lived or interrupted mass loss. For our models the default relative thickness is equal to 1000.

3.4 Results

3.4.1 Effects of Varying Mass-Loss Rate

As mentioned in the introduction, AGB stars throw off large amounts of matter into space when convection currents dredge the contents of the helium-burning shell up to the surface. Stars, however, do not necessarily lose mass at a constant rate. There may be episodes of increasing, decreasing or constant mass loss. These conditions can be modeled using DUSTYs radial dust distribution. Because the surface area of a sphere is $A = 4\pi r^2$, we can see that a constant mass-loss rate will incur a dust density distribution which is proportional to $1/r^2$. If density $\rho(r) \propto r^{-q}$, where q is the radial density parameter, we can say that when $q > 2$, the mass-loss rate of the star is increasing, while $q < 2$ indicates that the mass-loss rate is decreasing. This is important in determining the formation pressures and the relative abundances of various minerals as well as the resulting spectra (see e.g. Dijkstra et al. 2005).

Work by Marengo et al. (1999) suggests that many dust shells are not spherically symmetric but become increasingly spherical at larger distances from the star. Ueta (2002) agreed, finding that AGB stars have spherical outer shells but highly axisymmetric mass-loss towards the end of their time on the asymptotic branch. The cause of this is unknown (see Speck & Dijkstra 2006 in prep). Marengo et al. (2001) also found that some dust shells exhibit lowered dust shell temperatures, possibly indicating a recent decrease in the mass-loss rates in semiregular variable stars. For these reasons it is necessary to examine the effects of changing dust density distributions, which are caused by changes in mass-loss rate.

An interesting result is that as the radial density parameter q (from the dust density distribution $\rho(r) \propto r^{-q}$) is increased, spectral features of longer wavelength decrease in prominence as those of shorter wavelength increase. This would indicate that we would expect to see shorter wavelength features with greater relative intensities with increasing mass-loss rates, while the longer wavelength features become more prominent with decreasing mass-loss rates. (See Fig. 3.8.) Also, as the radial density parameter q decreases, a 26 μm feature becomes visible. This feature is not very prominent but still detectable at $q = 2$ with 20% silica, 80% warm silicates. Because this model utilizes spheroidal grains, it is unlikely that the 26 μm feature would be shifted any farther longward with other grain shapes, considering our experience with modeling corundum and spinel. This 26 μm feature increases in intensity with increasing optical depth (Fig. 3.9).
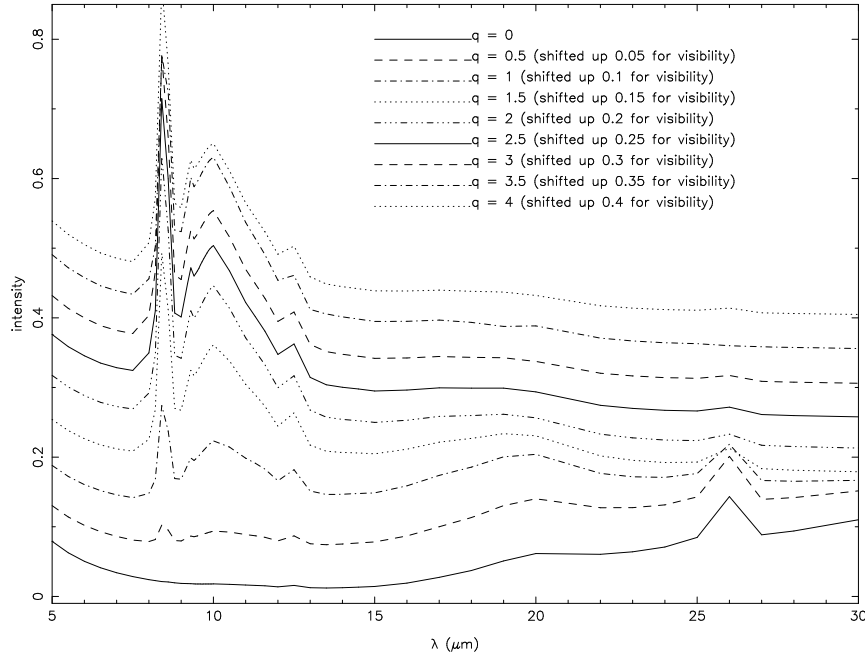
Figure 3.8: *A comparison of the output from models of a 20% spheroidal silica mixture at various dust density parameters q. Optical depth is set at $\tau_{10\mu m} = 0.05$.*
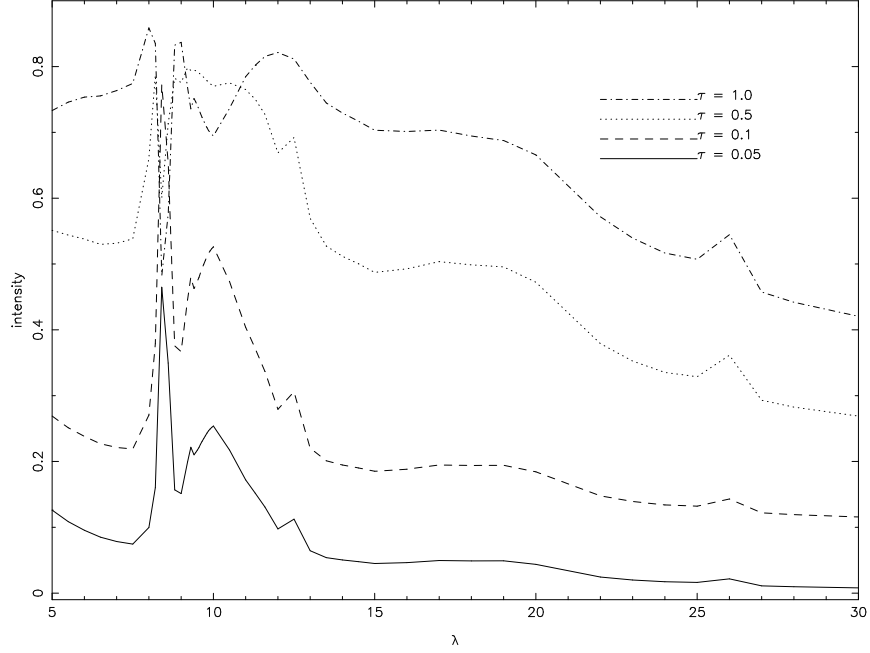
Figure 3.9: *A comparison of modeled spectra with differing optical depths. Note the change in prominence of the 26 μm feature.*

Sloan et al. (2003) found strong correlations between the 13 μm feature and two others at 20 and 28 μm. The long wavelength peak for quartz appears shortward of 28 μm, even for spheroidal grains. The resonance at these wavelengths leads us to believe that cristobalite or tridymite might have their resonance at the correct wavelength to explain the correlation between the 13 and 28 μm features in observed spectra. However, we lack optical constants n and k for longer wavelengths for tridymite and cristobalite, which precludes the analysis of grain shape effects.

In our models, there is also a broad 20 μm feature that appears with the 26 μm feature. For the lowest concentrations of silica (20% by mass), this feature grows in relative intensity as q decreases across all optical depths[13]. At the same time, the 9, 10 and 13 μm features

---
[13]Other relative abundances were not modeled but we expect a similar trend.

58

decrease in intensity. Thus, if mass loss is decreasing, then we should see a 20 and a 26 μm feature. If mass-loss is not decreasing, but is close to constant, the silicate features and the 13 μm feature will dominate. This would suggest that if quartz were responsible for the 13 μm feature, its strength would be greatly diminished in stars with decreasing mass loss. It also indicates that we may not necessarily observe a 20 or 26 μm feature with that at 13 μm. Spectra from Sloan et al. (2003) show a very broad feature between 16 and 22 μm (see Fig. 3.10). Thus it may be possible for the 20 μm feature to contribute to this broad 16-22 μm feature. These two features may not be separable in observational spectra.

When q is held constant at 2 (i.e. mass-loss rate is constant), the 13 μm feature of quartz starts to self-absorb at optical depths $\tau_{10\mu m} = 1$ in all cases studied ($\geq 20\%$ silica). For an optical depth of $\tau_{10\mu m} = 0.05$, as Ramdani (2003) postulates for Miras and SRs, there are still visible 20 and 26 μm features for a 20% silica mixture. The models seem to indicate that the 20 and 26 μm features will almost always appear together. However, as relative abundance increases, the 20 μm feature does become sharper and more prominent.

3.4.2   Effect of Grain Size

Grain size had little effect on the modeled spectra. As grain size increased, the features became stronger with one exception. The $\sim 9\mu$m feature goes into absorption at $\tau=0.5$ when silica makes up 40% of the dust mass and warm silicate comprising the remainder (see § 3.3.2).
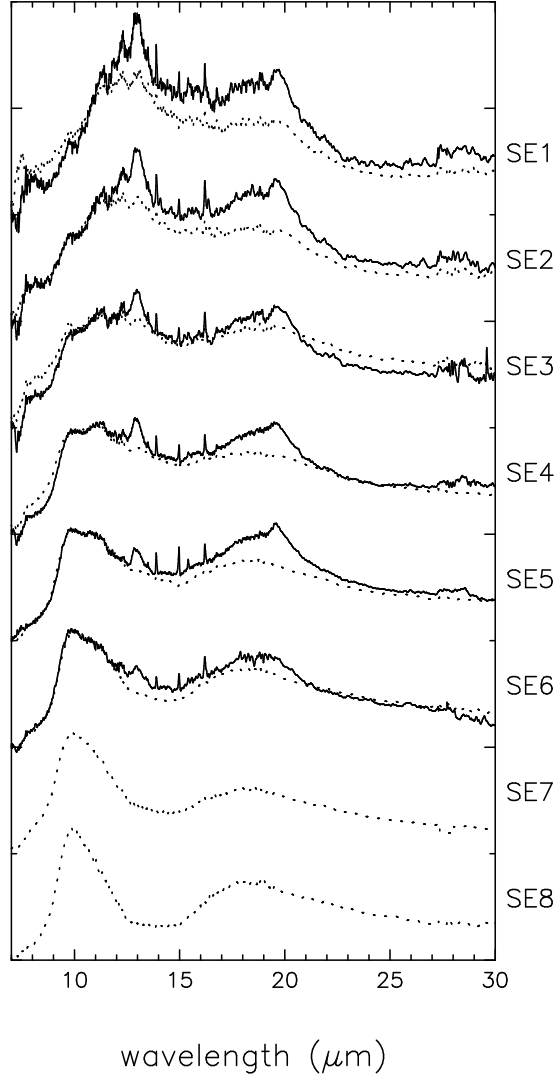
Figure 3.10: *Averaged spectra of silicate emission classes with (solid line) and without (dashed line) the 13 μm feature from Sloan et al. (2003). See § 3.4.5 for a discussion of these classes.*

3.4.3 Effects of Optical Depth and Composition

For four compositions we have modeled the effect of increasing optical depth. In all cases, the 13 μm feature increases in strength through $\tau_{10\mu m} = 0.5$, but then goes into absorption before optical depth reaches $\tau_{10\mu m} = 1$. The 8.5 μm feature, on the other hand, increases in strength at all relative abundances up to $\tau_{10\mu m} = 0.1$, but goes into strong absorption before it reaches

0.5. The 10 μm "classic" silicate feature, up to a 60% silica composition (Fig. 3.12), goes into absorption at $\tau_{10\mu m} = 0.5$. However, at 80% silica, the feature remains in emission even up to $\tau_{10\mu m} = 1$ (see Fig. 3.11). The broad 16-22 μm feature is only "broad" at concentrations of 20% or 40% silica (see Fig. 3.13 and 3.14) and at optical depths $\tau_{10\mu m} \sim 0.1$. Above 40% silica and optical depths greater than 0.1, the feature begins to peak more narrowly around 20 μm. The 26 μm feature is fairly weak at low silica concentrations and optical depths, as can be seen in Figure 3.14; however it becomes very large as these two variables increase. None of our models show this feature in absorption. If a different polymorph of silica shifts this feature to 28 μm, then it could possibly be a very prominent feature. However, the intensity of the 26 μm feature is more or less always comparable in size to the broad feature centered around 19 μm. The only exception to this seems to be our 20% silica mixture at optical depths of τ=0.05 and 1. Here the 26 μm feature is about half the size of the 20 μm feature. This 26 μm feature might prove to be well-correlated with the broad 16-22 μm bump, as Sloan et al. (2003) found with the 28 μm feature. However, Sloan et al. (2003) found that the extracted 28 μm feature was about half the size of the 20 μm feature. More laboratory data is needed to see if this 26 μm feature of quartz can be shifted to 28 μm by tridymite or cristobalite.

It would also be pertinent to note here that other oxides such as MgO and FeO may play a role in producing the observed spectra. Ferrarotti & Gail (2003) suggest that mag-nesiowustite ($Mg_{1-x}Fe_xO$) may form in small amounts in non-equilibrium reactions. This would create a feature somewhere between 15 and 20 μm. The precise location depends on the value of x. If a range of magnesiowustite compositions were present, a broad 15-20 μm

Figure 3.11: *A comparison of modeled spectra with differing optical depths. All models are comprised of 80% silica.*
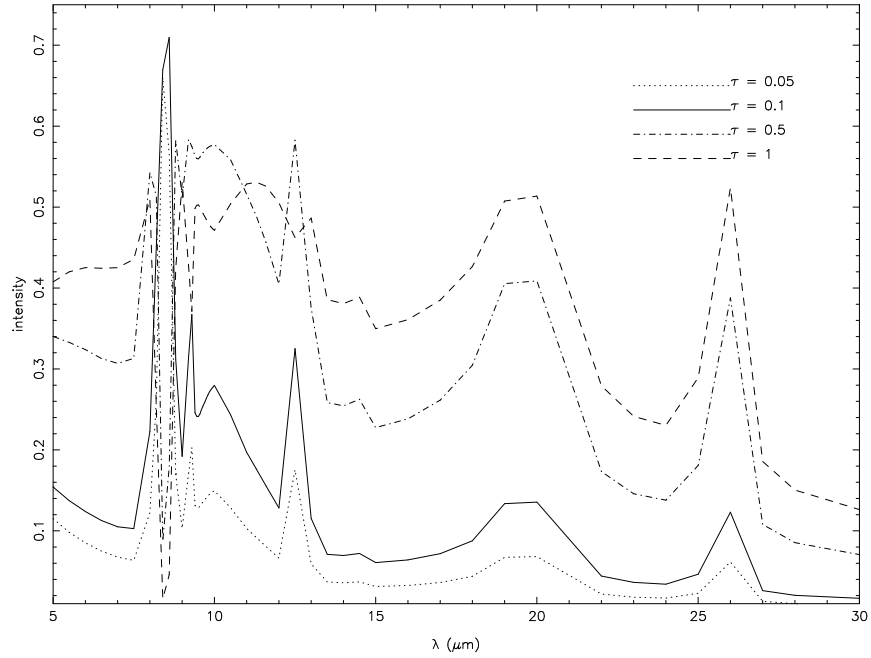
Figure 3.12: *A comparison of modeled spectra with differing optical depths. All models are comprised of 60% silica.*
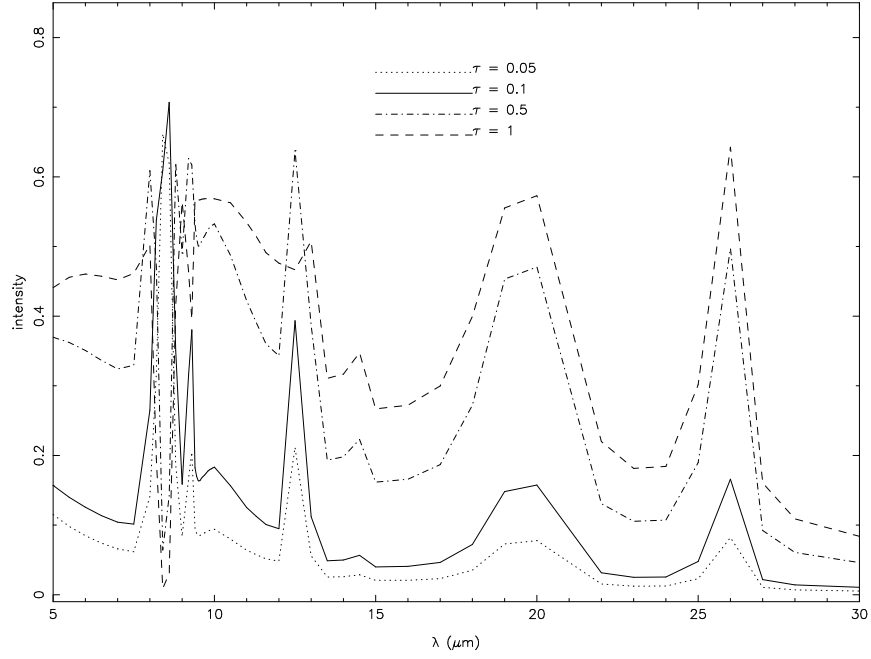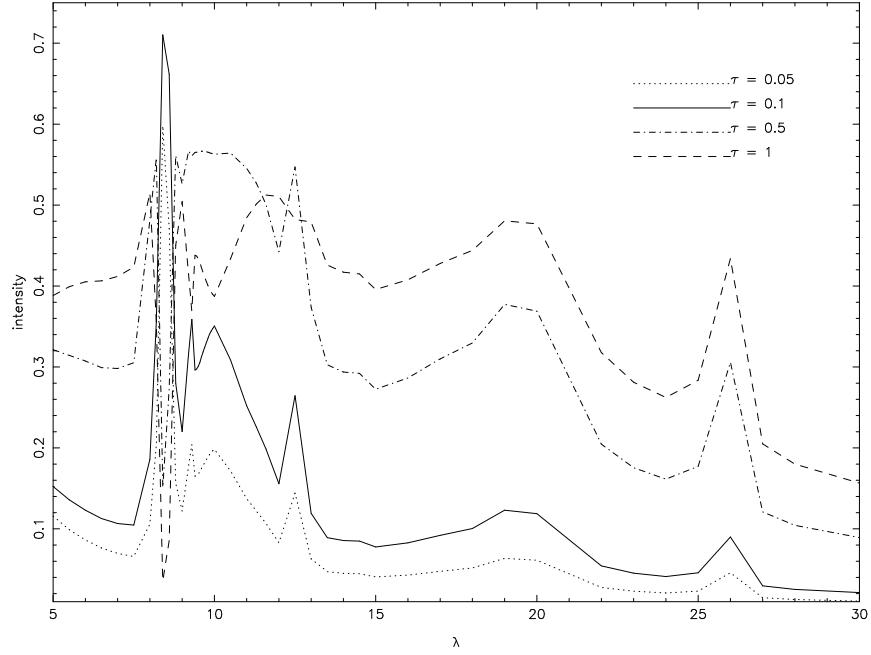
Figure 3.13: *A comparison of modeled spectra with differing optical depths. All models are comprised of 40% silica.*
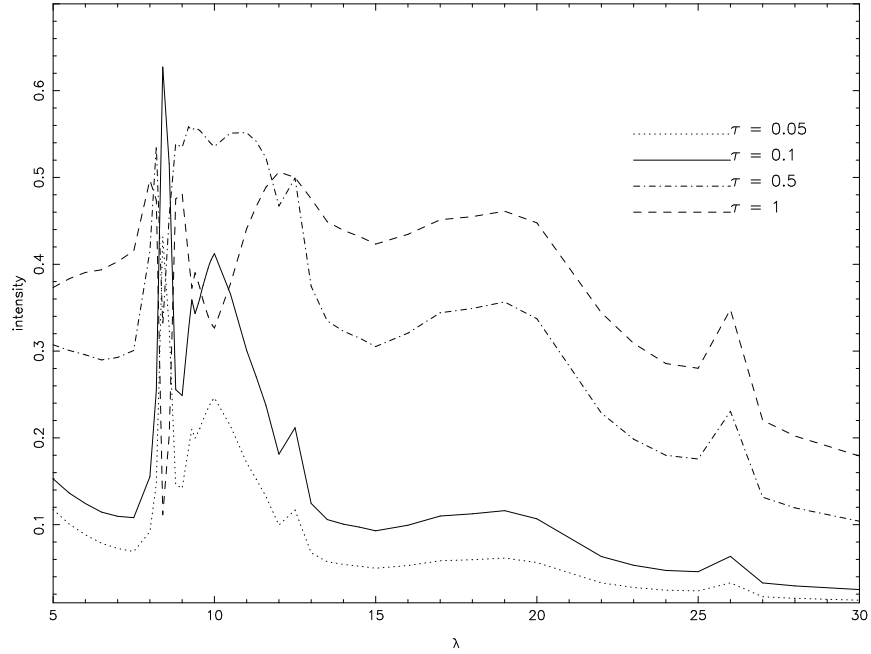
Figure 3.14: *Same as Figure 3.11, but for 20% silica mixtures.*

feature would be seen. Also, Rietmeijer et al. (1999) state that only a small amount of silica, MgO and FeO form in experimental gas-to-solid condensation. Thus, we should not

expect a high relative abundance of silica or magnesiowustite, but these two components could together contribute to a broad 16-22 μm feature.

3.4.4 Effect of Relative Dust Shell Thickness

Changing the relative dust thickness does not change the feature strength for most of the modeled output spectra (see Figures 3.15, 3.16, 3.17). We have also modeled the effect of relative thickness on a fixed optical depth and composition in Figure 3.18. For the most part the relative thickness does not significantly alter the spectra. However, there is one interesting effect: as relative thickness increases, the features in the 7-13 μm range quickly decrease in intensity when the mass-loss rate is rapidly decreasing ($q \leq 1$). This variable cannot then be related to the appearance or disappearance of the 13 μm feature because the 9 and 11 μm features are still present when the 13 μm feature is not observed. Therefore, better fits to astronomical data might be obtained by decreasing q and thus diminishing the features at 13 μm and shorter wavelengths.

3.4.5 Comparison to *ISO* Data

There are too many degeneracies in our modeling parameters to make good fits with the quartz models. Therefore we shall proceed with a qualitative discussion of our results.

Spectra from *ISO* for each of the silicate emission classes can be seen in Figure 3.10 from Sloan & Price (1995). The silicate emission classes, as mentioned previously, are assumed to serve as a measure of the relative silicate abundance in circumstellar dust shells. A lower number corresponds to strong emission by amorphous alumina and weak emission from
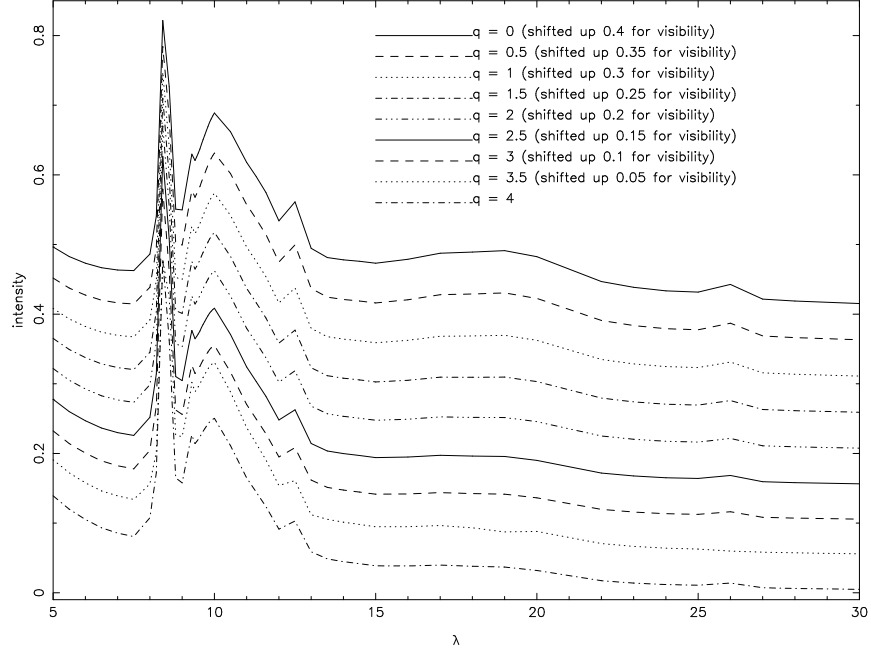
Figure 3.15: *A comparison of modeled spectra at varying dust density distributions, all set at a relative thickness of 10.* $\tau_{10\mu m} = 0.05$ *and relative abundance is 20% silica in all cases.*
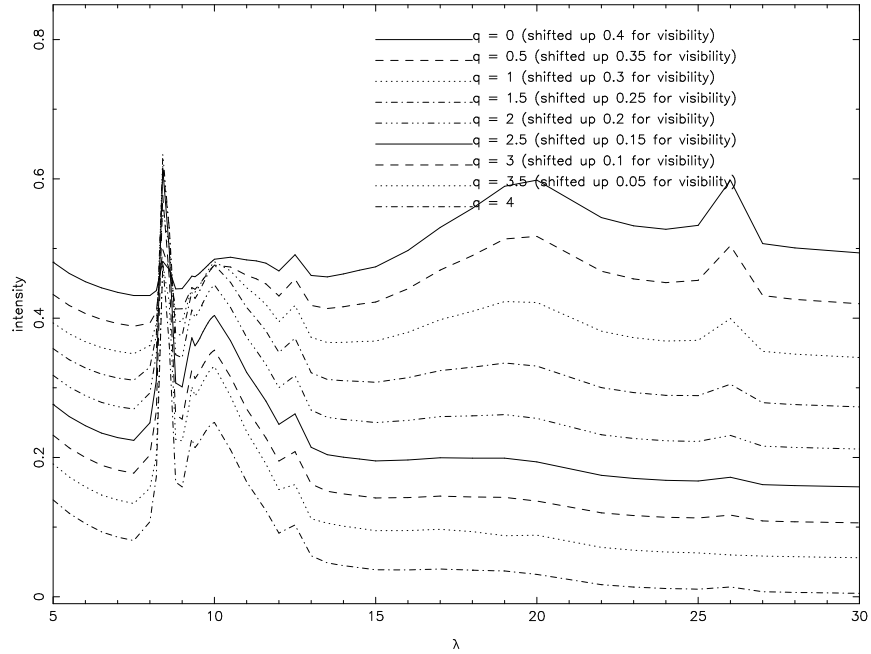
Figure 3.16: *Same as Figure 3.15, but here relative thickness is set at 100.*

silicates. Conversely, a higher number could indicate a lesser contribution from amorphous alumina and a stronger contribution from silicates (Speck et al. 2000).
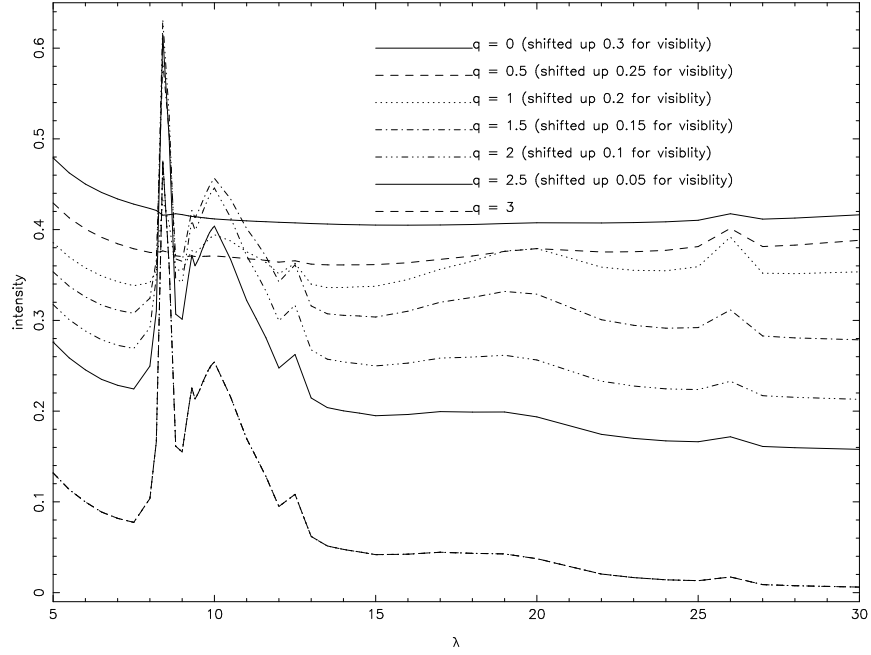
Figure 3.17: *Same as Figure 3.15, but here relative thickness is set at 10000.*
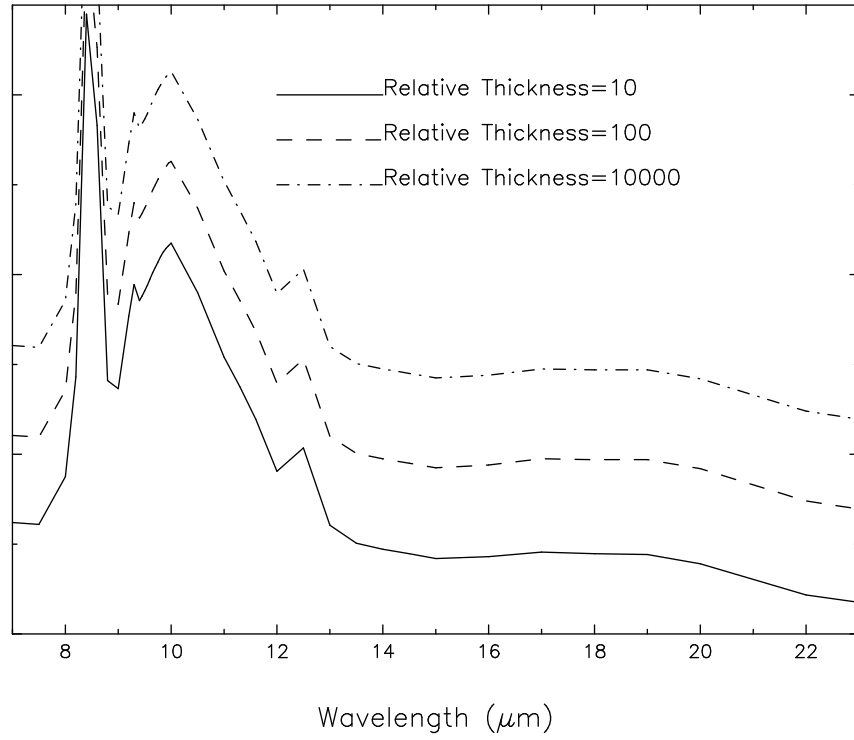
Figure 3.18: *Effect of relative thickness on modeled output spectra. Here we model a 20% quartz mixture at $\tau_{10\mu m} = 0.05$. The dust density parameter q is equal to 2.5.*

Higher concentrations of silica and optical depths tend to sharpen the 19 μm feature and push the 8.5 μm feature into absorption. In observations at 8.5 μm, no large features are found. Our models suggest that different mass-loss rates could alter the relative strength of the 13 and 19 μm features (see Figure 3.8). If mass loss decreases, the ratio of the 13/19 μm features will decrease. Likewise, if mass loss is increasing, the 13/19 μm ratio will increase. However, the longer wavelength features that become more noticeable in observational spectra seem to peak at wavelengths that are significantly longer. Although some overlap does occur, the quartz models do not match sufficiently to claim with any certainty that quartz is responsible for these features.

As mentioned above, Sloan et al. (2003) found a strong correlation between the 13 μm feature and features at 20 and 28 μm. The 19-20 μm feature of quartz increases somewhat in sharpness as SE number decreases. Its observation, however, would depend on whether or not this feature can be separated from the broad 16-22 μm feature. Tridymite and cristobalite both seem to peak more solidly at the 20 μm wavelength than quartz. Cristobalites feature at this wavelength is much more pronounced.

The prominence of the 8.5 μm feature is problematic. Because this feature goes into absorption in the range $0.1 < \tau < 0.5$ for all relative abundances, it would thus require circumstellar dust shells of significantly greater optical depth than that postulated by Ramdani for Mira and SR stars ($\tau=0.05$; Ramdani 2003). Alternatively, if the inner dust shell temperature were raised to 1000 K or above, we could possibly see this feature diminish, leaving the other features relatively intact, as noted in § 3.3.2. However, our models still fail to match the shorter wavelengths well. Optical depths and relative abundances well above

the expected ranges are needed to match the slope to the short wavelength side of the 13 μm feature.

We conclude that, given our difficulty in matching our models to observations, quartz may not be a good candidate for the 13 μm carrier. However, studies of tridymite and cristobalite have yet to be done, so other polymorphs of silica may yet yield good matches to the data.

3.5 Conclusion

There are several things to be gleaned from our models. First of all, because neither the 8.5 μm feature of quartz and cristobalite nor the 9 μm feature of tridymite appear in any star exhibiting the 13 μm feature, we must conclude that, if silica is truly the carrier, either optical depth is between τ=0.1 and 0.5 or else the silica could possibly form at a higher temperature. Furthermore, we have seen how increasing relative abundance of silica can sharpen the peak at 19 μm. Because of this, it would be possible to constrain the relative abundance expected for each silicate emission class. Also, given that SR stars do not necessarily exhibit constant mass-loss rates, one might further constrain the conditions for the specific SE classes by altering the radial density parameter q. By decreasing q, we can decrease the prominence of the shorter ($\leq$13 μm) wavelengths. By increasing q, we could decrease the prominence of the ($\geq$13 μm) longer wavelengths.

All this indicates that there will be degeneracies in the models; i.e. more than one model can give equally good results. We could say that either the lower numbered SE classes result from a dust shell that shows periods of decreasing mass loss or else there is an increased

relative abundance of silica present.

All crystalline polymorphs of silica exhibit the 13 μm feature. Though the 28 μm feature is not produced by quartz, another polymorph could potentially shift the 27 μm feature seen in non-spherical quartz grains to longer wavelengths.

If we assume a constant mass-loss rate (as argued in Rowan-Robinson & Harris 1982) and if quartz is the carrier of the 13 μm feature, it will probably be present at relative abundances $< 20\%$ unless there is another mineral species which can serve to mask the 20 and 26 μm features. Alternatively, if the 26 μm feature can be shifted to 28 μm by changes in crystal structure, this may explain the correlation between the 13 and 28 μm features.

Chapter 4: Discussion

In the course of this thesis, the cases for and against the 13 μm carrier candidates corundum, spinel and quartz have been examined. It is obvious from the modeling results that none of these species can completely explain the observed features. However, some trends have been identified, enabling one to draw some valuable conclusions.

Over the years, various possible carriers of the 13 μm feature have been proposed. Onaka, de Jong & Willems (1989) suggested aluminum oxide (alumina; Al_2O_3) as the source of the 13 μm feature, while it was later proposed that this species might be in the form of corundum (α-Al_2O_3; Glaccum 1995). Begemann et al. (1997), in their laboratory analysis of corundum, showed that in addition to the 13 μm feature, corundum possesses a weak feature at 21 μm. Since this 21 μm feature has not been observed in the spectra of astronomical sources which exhibit the 13 μm feature, Begemann et al. (1997) concluded that corundum could not be the carrier of the 13 μm feature. Begemann et al. (1997) also found a correlation between the 13 μm feature and the classic 10 μm feature and thus concluded that the carrier of the 13 μm feature must be some sort of silicate. However, Posch et al. (1999) stated that the strong 10 μm Si-O feature is not observed in the IRAS or ISO spectra of AGB stars which exhibit the 13 μm feature, contradicting the finding of Begemann et al. (1997). Kozasa &

Sogawa (1997, 1998) proposed grains consisting of Al_2O_3 cores and silicate mantles for the carrier of the 12.5-13.0 μm feature. However, this was investigated by Posch et al. (1999) who found that: 1) there would have to be a large population of grains of 85% Al_2O_3; and 2) there would have to be an even larger number of pure silicate particles to produce anywhere near the correct ratio of 13 μm to 10 μm flux strengths. They therefore concluded that such core-mantle grains were unlikely to be the carriers of the 12.5-13.0 μm feature. Because of the limitations of radiative transfer code, core-mantle grains are beyond the scope of the studies presented here.

Posch et al. (1999) suggested spinel ($MgAl_2O_4$) as the carrier of the 13 μm feature, noting that stoichiometric natural spinel also exhibits features at 16.8 and 32 μm. Posch et al. (1999) suggested that both the 16.8 and 32 μm features are observed in ISO SWS data for O-rich AGB stars which exhibit the 13 μm feature. However, Sloan et al. (2003) pointed out that the observed 16.8 μm feature is too narrow to be a dust feature and suggested it may instead be explained by the presence of CO_2, which is well-correlated with the 13 μm feature (Justtanont et al. 1998). Furthermore, they found no evidence for a 32 μm feature. Further studies of the ISO SWS spectra for stars which exhibit the 13 μm feature by Heras & Hony (2005) also failed to find a dust feature to match the spinel 16.8 μm spectral feature.

Silica (SiO_2) was first suggested as the carrier of the 13 μm feature by Speck (1998). Silicon dioxide is an anomaly amongst the oxides. Although SiO_2 is chemically an oxide, the structures and properties of the silica minerals are more closely allied to those of silicates (see Speck 1998). Posch et al. (1999) claimed that the lack of correlation between the 13 μm feature and the strong 10 μm feature expected for SiO_2 should rule silica out as the

carrier. However, as stated above, Begemann et al. (1997) did find a correlation between the 13 μm feature and the classic 10 μm feature and thus concluded that the carrier of the 13 μm feature must be some sort of silicate (which could include silica). It is possible that the objection of Posch et al. (1999) to this attribution was based on unusual optical constants. Their SiO_2 constants (from Henning & Mutschke 1997) produce an emission feature that is shifted to the blue side of the regular silicate feature. This is not seen for other SiO_2 optical constants (e.g. Spitzer & Kleinman 1961). Furthermore, silica has several possible crystal structures, each of which has a subtly different spectrum, such that the ratio of feature strengths of the 10 and 13 μm features vary substantially (see Speck 1998).

Our analysis of corundum and spinel in Chapter 2 suggests that, because these two minerals emit at the 13 μm wavelength only in the form of spherical grains, corundum and spinel must be in this form in order to be included in the list of carrier candidates. Our modeling results show that spinel can be excluded from this list, given its prominent 17 μm feature, which is not seen in observed spectra. On the other hand, because corundum is thought to form in hotter regions close to the star, it is plausible that corundum could form spherical grains and thus produce the 13 μm feature. However, spherical corundum grains have not yet been found in meteorites, although there is a possibility that this is due to the methods used to isolate the grains. This remains an important point that could ultimately decide the case for corundum.

While quartz can possess features at 13, 20 and 27 μm (in the case of non-spherical grains), our models for this species have provided lackluster results.

Although the 19 μm feature might become narrower with increasing relative abundance,

this narrowing may not be noticed due to the presence of MgO and FeO features in this same region. Magnesium and iron oxides (MgO and FeO) have been observed in the spectra of O-rich stars, indicating that thermodynamic equilibrium has not yet been reached. This also suggests that silica could persist around these stars, since silica is a result of non-equilibrium conditions. MgO and FeO are expected to combine with SiO_2 to form silicates in a system which has reached equilibrium.

It is possible to reduce the prominence of the 8.5 μm feature at high temperatures if the optical depth is sufficiently high ($\tau_{10\mu m} \gtrsim 0.5$). At $\tau_{10\mu m} = 0.05$, the optical depth speculated for Mira and semiregular variable stars (Ramdani 2003), the optical depth of the observed stars may be far too low to see this effect.

We have ruled out spinel as a carrier, but silica and corundum still remain candidates. Corundum shows the most promise, but it is still unclear why this mineral species should be associated with SR stars. Although quartz has not provided good matches to observations, more optical constants are needed to investigate tridymite and cristobalite. Silica is theoretically a good candidate because its association with SRs could be explained by dust formation in the less dense circumstellar shells. In this environment non-equilibrium chemistry may occur.

In future research, spatial correlation studies (spectro-imaging) should be pursued to determine which spectral features are spatially correlated. For instance, if SiO_2 is the carrier of the 13 μm feature, there will be a spatial correlation between the emission at 13 μm and that at 10 μm, since the laboratory spectrum of silica shows both these features. Such a correlation is not necessary if the carrier is corundum. Corundum forms at higher tempera-

tures than silicates or silica, suggesting that the signature of corundum will occur closer to the central star. Moreover, with increasing radial distance, corundum is expected to become coated with a mantle of the (much more abundant) silicate minerals, thus hiding its spectral features. Therefore, if the corundum produces the 13 μm feature, we would expect this feature to be confined to the region of the circumstellar shell closest to the central star. The silicates that dominate the spectra of these stars form by reacting SiO_2 with MgO and FeO (e.g. Rietmeijer et al. 1999, Lodders & Fegley 1999). If equilibrium is not reached, which may be possible in the less dense SR dust shells, residual SiO_2, MgO and FeO grains may exist in these circumstellar shells. In addition, CO_2 is known to be associated with stars that exhibit the 13 μm feature. Spatial correlation of this feature with those of CO_2 would constrain the formation temperature and aid our understanding of dust formation.

In addition to the observational possibilities, this subject would benefit from further radiative transfer modeling. In particular, including amorphous alumina and/or the Mg-Fe oxides in the silica (and corundum) models would be informative. Furthermore, 2-d modeling could also help improve upon our results.

References

Alexander, C.M.O'D., Nittler, L.R., Tera, F., 2001, Lunar Planet. Sci., 32, 2191.

Begemann, B., Dorschner, J., Henning, Th., Mutschke, H., Guertler, J., Koempe, C., Nass, R., 1997, ApJ, 476, 199.

Begemann, B., Henning, T., Mutschke, H., Dorschner, J., 1995, P&SS, 43, 1257.

Bohren, C.F. & Huffman, D.R., *Absorption and Scattering of Light by Small Particles*, New York: Wiley, 1983.

Cami, J., de Jong, T., Tielens, A.G.G.M., Justtanont, K., Waters, L.B.F.M., Yamamura, I., 1998, IAUS, 191, 230.

Chopelas A., Hofmeister A.M., 1991, Phys. Chem. Min., 18, 279.

Chylek, P., Videen, G., Geldart, D.J.W., Dobbie, J.S. & Tso, H.C.W., 2000, *Effective Medium Approximations for Heterogeneous Particles.* in Light Scattering by Non-spherical Particles, Theory, Measurements and Applications, ed. M.I. Mishchenko, J.W. Hovenier & L.D. Travis (San Diego: Academic Press), 273-308.

Clayton, D. & Nittler, L., 2004, ARA&A, 42, 39.

de Graauw, T. et al., 1996, AAP, 315, L49.

DePew, K., Speck, A.K., Dijkstra, C., 2006, ApJ, 640, 971.

Dijkstra, C, Speck, A.K., Reid, R.B., Abrahams, P., 2005, ApJ, 633L, 133.

Egan, M.P. & Sloan, G.C., 2001, ApJ, 558, 165.

Fabian, D., Posch, T., Mutschke, H., Kerschbaum, F., Dorschner, J., 2001, A&A, 373, 1125.

Feast, M.W., Whitelock, P.A., 1987, Lsse. Proc., 33.

Ferrarotti, A.S. & Gail, H.-P., 2003, A&A, 398, 1029.

Gervais, F. (1991) in Palik E. (ed) *Handbook of Optical Constants, II.* Acad. Press., p.761.

Gillett, F.C., Low, F.J., Stein, W.A., 1968, ApJ, 154, 677.

Glaccum, W., 1995, ASPC, 73, 395.

Hafner S., 1961, Z. Krist. 115, 331.

Henning Th., Mutschke H., 1997, A&A, 327, 743.

Henning, T. et al. 1995, A&AS, 112, 143.

Heras, A.M., Hony, S., 2005, A&A, 439, 171.

Hofmeister, A.M., Keppel. E. & Speck, A.K., 2003, MNRAS, 345, 16.

Hoppe, P., 2003, in *Astrophysics of Dust*, ASP Conference Series, Vol. 309, Eds. Adolf N. Witt, Geoffrey C. Clayton and Bruce T. Draine., p.265.

Huss G.R., Fahey A.J., Gallino R., Wasserburg G.J., 1995, ApJ, 430, L81.

Ivezic, Z., Nenkova, M. & Elitzur, M., 1999, User Manual for DUSTY, University of Kentucky Internal Report, accessible at http://www.pa.uky.edu/ moshe/dusty

Justtanont, K., Feuchtgruber, H., de Jong, T., Cami, J., Waters, L.B.F.M., Yamamura, I., Onaka, T., 1998, A&A, 330, L17.

Kemper, F. Waters, L.B.F.M., de Koter, A., Tielens, A.G.G.M., 2001, A&A, 369, 132.

Kerschbaum, F., Hron, J., 1992, A&A, 263, 97.

Kessler, M.F., 1995, SSRv, 74, 57.

Kessler, M.F. et al., 1996, A&A, 315, L27.

Kosaza T., Sogawa H., 1998, Ap&SS 255, 437.

Kosaza T., Sogawa H., 1997, Ap&SS 251, 165.

Little-Marenin, I.R. & Little, S.J., 1988, ApJ, 333, 305.

Little-Marenin, I.R. & Little, S.J., 1990, AJ, 99, 1173.

Little-Marenin, I.R. & Price, S.D., 1986, INPR Conf., 137.

Lodders, K. Fegley, B. Jr., 1999, in T. Le Bertre, A. Lèbre & C. Waelkens (eds) Asymptotic Giant Branch Stars, IAUS, 191, 279.

Maldoni, M.M., Ireland, T.R., Smith, R.G., Robinson, G., 2005, MNRAS, 362, 872.

Marengo, M., Busso, M., Silvestro, G., Persi, P., Lagage, P.O., 1999, A&A, 348, 501.

Marengo, M. Ivezić, Ž., Knapp, G.R., 2001, MNRAS, 324, 1117.

Mathis, J.S., Rumpl, W., Nordsieck, K.H., 1977, ApJ, 217, 425.

Messenger, S., & Bernatowicz, T.J., 2000, Meteorit. Planet. Sci., 35, A109.

Messenger, S., Keller, L.P., Stadermann, F.J., Walker, R.M., & Zinner, E., 2003, Sci, 300, 105.

Min, M., Hovenier, J.W., de Koter, A., 2003, A&A, 404, 35.

Min, M., Hovenier, J.W., de Koter, A., 2005, A&A, 432, 909.

Neugebauer, G. et al., 1984, ApJ, 278, L1.

Nenkova, M., Ivezic, Z., & Elitzur, M., 2000, ASPC, 196, 77.

Neugebauer, G. et al., 1984, ApJ, 278, L1.

Nittler, L.R., Alexander, C.M.O'D., Gao, X., Walker, R.M., Zinner, E.K., 1997, ApJ, 483, 475.

Nittler, L.R., Alexander, C.M.O'D., Gao, X., Walker, R.M., Zinner, E.K., 1994a, Nature, 370, 443.

Nittler, L.R., Alexander, C.M.O'D., Gao, X., Walker, R.M., Zinner, E.K., 1994b, Meteoritics Planet. Sci. 29, 512.

Onaka, T., de Jong, T., Willems, F.J., 1989, A&A, 218, 169.

Ossenkopf, V., Henning, Th., Mathis, J.S., 1992, A&A, 261, 567.

Pagel, B.E.J., *Nucleosynthesis and Chemical Evolution of Galaxies*, Cambridge, UK: Cambridge University Press, 1997. Posch, T., Kerschbaum, F., Mutschke, H., Fabian, D., Dorschner, J., Hron, J., 1999, A&A, 352, 609.

Preudhomme J., Tarte P., 1971, Spectrochimica Acta 27A, 1817.

Ramdani, A., 2003, EIDA Conf., 145.

Rietmeijer, F.J.M., Nuth, J.A., Karner, J.M., 1999, ApJ, 527,395.

Rowan-Robinson, M, Harris S., 1982, MNRAS, 200, 197.

Rowan-Robinson, M., Harris S., 1983a, MNRAS, 202, 767.

Rowan-Robinson, M., Harris S., 1983b, MNRAS, 202, 797.

Salpeter, E.E., 1974, ApJ, 193, 579.

Sedlmayr, E., 1997, Ap&SS, 251, 103.

Sloan, G.C., Price, S.D., 1995, ApJ, 451, 758.

Sloan, G.C., Price, S.D., 1998, ApJS, 119, 141.

Sloan, G.C., Levan, P.D., Little-Marenin, I.R., 1996, ApJ, 463, 310.

Sloan, G.C., Kraemer, K.E., Goebel, J.H., Price, S.D., 2003, ApJ, 594, 483.

Speck, A.K., PhD thesis, 1998.

Speck, A.K., Barlow, M.J., Sylvester, R.J., Hofmeister, A.M., 2000, A&AS, 146, 437.

Spitzer, W.G., Kleinman, D.A., 1961, Phys. Rev., 121, 1324.

Stevens, S.J., Hand, R.J., & Sharp, J.H., 1997, Journal of Materials Science, 32, 11, 2929.

Stroud, R.M., Nittler, L.R., Alexander, C.M.O'D., 2004, Sci, 305, 1455.

Tielens, A.G.G.M., Waters, L.B.F.M., Molster, F.J., Justtanont, K., 1997, Ap&SS, 255, 415.

Tielens A.G.G.M., 1990, in *From Miras to Planetary Nebulae: Which Path for Stellar Evolution?* Proceedings of the International Colloquium, Montpellier, France. Gif-sur-Yvette, France: Éditions Frontières, p. 186.

Ueta, T., 2002, PhD Thesis.

Vardya, M.S., de Jong, T.,Willems, F.J., 1986, ApJ, 304, L29.

Voshchinnikov, N.V. & Semenov, D.A., 2000, AstL, 26, 679.

Warren, J.L., Barret, R.A., Dodson, A.L., Watts, L.A. & Zolensky, M.E., eds. 1994, Cosmic Dust Catalog, Vol. 14, NASA Johnson Space Center, Houston.

Woolf N.J., Ney E.P., 1969, ApJ 155, L181.

Zinner, E., Amari, S., Guinness, R., Nguyen, A., Stadermann, F. J., Walker, R. M., Lewis, R. S., 2003, GeCoA, 67, 5083.